Journal of Electrical Engineering & Technology
https://doi.org/10.1007/s42835-026-02687-y

ORIGINAL ARTICLE

# Solar Irradiation Prediction Using Time Series Models: Performance Evaluation with Hyperparameter Optimization and K-Fold Cross-Validation

**Faruk Ayata**[1] · **Ebubekir Seyyarer**[2] · **Erşan Ömer Yüzer**[3]

Received: 19 December 2024 / Revised: 9 January 2026 / Accepted: 5 February 2026
© The Author(s) under exclusive licence to The Korean Institute of Electrical Engineers 2026

**Abstract**
Solar irradiation prediction is a very important topic for the regions where solar energy systems will be established and for investment policies to be made in the coming years for these increasingly popular systems. However, the continuous change in solar irradiation due to time and atmospheric conditions necessitates developing and evaluating different prediction models. This study aims to assess and analyze the prediction performance of global solar irradiation on a horizontal plane using different time series algorithms, based on meteorological parameters obtained historically and seasonally in Hakkâri, Türkiye, which has a high solar energy potential, between 2019 and 2022. In this context, Autoregressive Integrated Moving Average (ARIMA), Seasonal Autoregressive Integrated Moving Average (SARIMA), Simple Exponential Smoothing (SES), and Holt-Winters Exponential Smoothing (HWES) models are preferred as time series-based solar irradiation prediction models. The study presents a comparative analysis based on the results obtained among the time series algorithms used as prediction models. It details their applications and determines the potential of solar irradiation prediction models. The performance of each prediction model is compared using performance evaluation criteria commonly used in the literature. To increase the success of the models, Grid Search optimization algorithm for hyperparameter optimization and K-Fold cross-validation method for the acceptability of the results are used. It is observed that the success rates of the optimized models are significantly increased compared to their standard forms. The results indicate that the proposed time series models, in terms of evaluation criteria, show that ARIMA and SARIMA models yield successful results and SES and HWES models yield approximately similar results. Overall, this study presents a comprehensive view of time series models that can be used to improve solar irradiation prediction.

**Keywords** Solar irradiation · Time series · Prediction · Performance evaluation · Hyperparameter optimization · K-Fold cross-validation

## 1 Introduction

The climate crisis affecting the entire world and energy disputes among countries are increasing interest in renewable energy systems daily. In this context, the increasing development of photovoltaic (PV) technology highlights the importance of prediction studies related to solar irradiation, which is the most critical parameter for these systems. However, solar energy's non-stationary nature and complexity significantly complicate prediction studies.

In many regions worldwide, mainly rural areas, no devices measure solar irradiation due to installation, maintenance, and calibration requirements [1]. Therefore, predicting solar irradiation using meteorological parameters is

✉ Faruk Ayata
farukayata@yyu.edu.tr

Ebubekir Seyyarer
eseyyarer@yyu.edu.tr

Erşan Ömer Yüzer
ersanomeryuzer@hakkari.edu.tr

[1] Başkale Vocational High School, Van Yüzüncü Yıl University, Van 65090, Türkiye

[2] Computer Engineering, Van Yüzüncü Yıl University, Van 65090, Türkiye

[3] Çölemerik Vocational High School, Hakkâri University, Hakkâri 30100, Türkiye

Published online: 02 March 2026

of great importance [2]. From this perspective, researchers have developed many models for solar irradiation prediction studies to date, achieving successful prediction results. Among these models, those based on mathematical formulas (empirical) are frequently used and produce effective solar irradiation prediction results [3–8]. However, these models do not reflect complex and non-linear relationships as they do not include some meteorological parameters (such as wind speed, atmospheric pressure, etc.) in the calculations [9]. On the other hand, solar energy is influenced by various meteorological factors and exhibits highly complex, non-linear properties. These complexities in solar data encompass spatial and temporal elements, which are effectively captured by deep learning (DL) models [10]. Therefore, different artificial intelligence models based on DL have started to be used in solar irradiation prediction studies, as in many engineering fields. Studies show that more accurate prediction results are obtained using these models than empirical ones [11, 12]. DL models outperform machine learning (ML) models in time series-based prediction problems [13]. This study evaluates the performance of time series models in solar irradiation prediction.

### 1.1 Review of Literature

ARIMA models are widely used in energy systems due to their versatility and simplicity. ARIMA has high accuracy, especially for predicting solar irradiation based on ground-based measurements [14, 15]. Dazhi et al. applied the ARIMA model to predict hourly solar irradiation, factoring in the effects of cloud cover. Their research, which utilized data from two weather stations in the USA, demonstrated that incorporating cloud cover information enhances prediction accuracy [16]. Belmahdi et al. compared the Autoregressive moving-average model (ARMA) and ARIMA models to predict the monthly average daily global solar irradiation in Tetouan, a city in northern Morocco. The results indicated that the ARIMA model outperformed ARMA regarding prediction success [17]. Chodakowska et al. explored the use of ARIMA models for seasonal solar irradiation prediction in Jordan and Poland, two countries with differing climatic conditions. Their findings suggest that ARIMA models are effective for solar irradiation prediction and could support the long-term stable integration of solar energy into national grids [18].

SARIMA is a successful alternative that includes the seasonal part of the ARIMA model [19]. Alsharif et al. developed a SARIMA model to predict daily and monthly solar irradiation in Seoul, South Korea, using hourly solar irradiation data obtained over 37 years from the Korea Meteorological Administration. They showed that the developed model succeeded in predicting solar irradiation [20]. Kardakos et al. proposed a SARIMA-based model using solar irradiation data to predict a solar energy plant's hourly PV output power. The study achieved successful predictions with an 11.12% normalized root mean square error (nRMSE) value [21]. Bouzerdoum et al. used a hybrid model based on SARIMA and Support Vector Machine (SVM) for hourly power generation prediction of a solar power plant. They showed that the hybrid model was more efficient than models using SARIMA and SVM alone [22].

Although many different solar irradiation prediction methods are proposed in the literature besides ARIMA and SARIMA, the SES method is still widely used for modeling time series analyses in this field [23]. SES methods are simple and accurate prediction models, but their performance largely depends on the values of the smoothing parameters [24]. The main advantage of this method is its robustness, which allows the technique to be applied quickly and effectively along with descriptive and inferential statistics [25]. Wu et al. conducted a study to predict hourly global solar irradiation employing various techniques, such as the exponential smoothing state-space model (ESSS), ARIMA, linear exponential smoothing (LES), SES, and random walk (RW), using data collected in Singapore. Their findings revealed that ESSS outperformed the other methods for prediction intervals ranging from 5 to 20 min [26]. Pacurar et al. conducted a solar irradiation prediction study using RW, LES, and SES methods with data recorded at 15-second intervals in Timisoara, Romania, in 2009 and 2010. They found that the RW model performed the best [27]. Azimi et al. introduced a novel hybrid model for predicting solar irradiation incorporating the k-means algorithm. They compared the outcomes with various models, including SES and ARIMA methods. The results showed that the proposed hybrid model provided higher accuracy than the other models [28].

Modifying the previous method is necessary when there are components such as trend or seasonality in variables like direct normal irradiation (DNI) and global horizontal irradiation (GHI). The best method including these components is Holt-Winters [29]. This method is not very commonly used in solar irradiation prediction studies but is widely used in energy demand, production, and consumption studies, offering high accuracy, especially for energy production prediction [30–33]. Prema and Rao proposed time series models, including Holt-Winter and SES methods, for short-term (1 day) solar irradiation prediction using data collected from Bagalkot meteorological station in Karnataka, India, between 01/01/2012 and 30/05/2013. The developed models could accurately predict the next day's solar irradiation [34]. Dhingra et al. evaluated several time series methods, including seasonal autoregressive integrated moving average exogenous (SARIMAX), ARIMA, Holt-Winters, and

autoregression (AR), to forecast solar energy production in household solar energy systems. After implementing various preprocessing techniques, they discovered that the Holt-Winters method provided the closest predictions to the actual solar energy values in cumulative time series prediction, with a root mean square error (RMSE) of 5.3949 [35]. Bushirat and Ismaila conducted a study on solar irradiation prediction using solar irradiation data covering Nigeria from January 2003 to December 2016. They predicted solar irradiation with five different methods, including Holt-Winters and SARIMA. The results obtained from the applied prediction methods were above average [36].

Beyond traditional statistical methods, recent literature has focused on deep learning and graph neural networks (GNNs) for modelling complex, nonlinear and spatio-temporal dependencies, particularly in renewable energy and load forecasting. In this context, models such as Spatio-Temporal Graph Networks (STGNN and STDGAT) have been proposed to improve forecast accuracy for wind farm clusters (WFCs) and large-scale photovoltaic clusters [37–38]. These advanced approaches improve forecasting performance by correcting errors in Numerical Weather Prediction (NWP) data or modelling the effects of inter-station dynamic spatial convergence (SFACED). GNNs and new feature extraction techniques, such as CNN-LSTM hybrid models and EIIR, are also used to recognise morphological features, such as peaks and valleys, in load forecasting [39]. This trend also encompasses innovative, problem-specific modelling strategies. For instance, distribution regression methods have been developed for telecommunications reliability prediction, estimating the distribution of the relevant KPI rather than the metric itself [40].

Furthermore, studies have employed structured analysis techniques such as the integrated ISM-Fuzzy MICMAC approach to assess complex, interrelated factors affecting model performance in industrial contexts [41]. This highlights the broader applicability of meta-model optimization strategies, similar to grid search and cross-validation used in this study.

In addition to predictive models, optimising and planning energy systems remains a critical area of research. Metaheuristic optimization techniques have been successfully applied to enhance energy-related decision-making systems [42]. Examples of these approaches include the use of multi-objective genetic algorithms to solve problems at different scales, such as the long-term capacity optimisation of multi-energy bases (wind, photovoltaic, and thermal) [43] and the thermodynamic optimisation of solar power tower (SPT) systems [44]. Optimization is used not only for capacity planning, but also for uncertainty management. In the planning of shared energy storage in industrial parks, for instance, two-layer hybrid frameworks such as Robust Information Gap Decision Theory (IGDT) for handling uncertainty and Distributed Model Predictive Control (DMPC) for real-time operation have been proposed [45].

In addition to prediction-oriented studies, recent research has also focused on improving the performance of photovoltaic systems using advanced control strategies that consider system uncertainties and dynamic conditions [46, 47]. These studies emphasize the importance of accurate solar irradiation data, as it directly affects the reliability of PV system control and energy management.

In addition to studies focused on prediction, recent research has also concentrated on enhancing the performance of photovoltaic systems by employing advanced control strategies that consider system uncertainties and dynamic conditions [46, 47]. Current approaches in this area integrate prediction mechanisms directly into control loops. One example is the improved Power-to-Place (MPPT) algorithm, which suppresses power oscillations and increases tracking speed using two-stage power prediction [48]. Alongside control strategies, there is also practical applied research focusing on experimental performance analyses of innovative systems, such as the PV-Trombe Wall, which combines heating, power generation and air purification applications [49]. Both algorithmic approaches that improve control efficiency and practical analyses that verify the real-world performance of systems strongly emphasise the importance of accurate solar irradiation data, as this directly impacts the reliability of PV system control and energy management.

### 1.2 Motivation of the Study and Present Research Contributions

The increasing importance of renewable resources in today's energy policies highlights the necessity of predicting the efficiency of solar energy production in advance. In this context, the need to develop solar irradiation forecasting models based on simple and commonly measured meteorological parameters motivates the development of cost-effective and practical approaches. Furthermore, considering traditional models' limitations in data acquisition and computational costs due to their complex structures, models based on simpler input data emerge as an essential research area with the potential to provide reliable predictions.

In this study, solar irradiation forecasting was conducted using time series models such as ARIMA, SARIMA, SES, and HWES based on key meteorological parameters (atmospheric pressure, ambient temperature, relative humidity, and wind speed). The results obtained were compared with similar studies in the literature, as presented in Table 1. The table comprehensively compares studies conducted in

**Table 1** Comparison of the time series models used in this study with those employed in other studies

| Ref. | Study location | Prediction Model | Data Parameters | Time Scale | Performance metrics used |
|---|---|---|---|---|---|
| [20] | Seoul, South Korea | SARIMA | Solar irradiation (Wh/m$^2$) | Daily Monthly | $R^2$, RMSE |
| [50] | New Delhi/India | ARIMA | Solar irradiation (kWh/m$^2$) | Monthly | $R^2$, RMSE, MAE, MAPE |
| [51] | Tetouan and Tangier, Morocco | ARIMA | Ambient temperature (°C) Relative humidity (%) Wind speed (m/s) Solar irradiation (kWh/m$^2$) Geographical coordinates (°) | Daily | $R^2$, RMSE, MBE |
| [52] | Utrecht, Hollanda | HWES | Solar irradiation (W/m$^2$) | Hourly | $R^2$, MAE |
| [53] | 6 different cities, Türkiye | ARIMA, SARIMA | Ambient temperature (°C) Relative humidity (%) Solar irradiation | Hourly | R, RMSE, MAE |
| [54] | Şanlıurfa, Türkiye | ARIMA SES HWES | Ambient temperature (°C) Relative humidity (g/m$^3$) Wind speed (m/s) Solar irradiation (W/m$^2$) | Daily | RMSE, MAE, MSE, nRMSE |
| [17] | Tetouan, Morocco | ARIMA | Solar irradiation (kWh/m$^2$) | Monthly | RMSE, MAPE, MBE |
| [55] | Awali, Bahrain | ARIMA | Ambient temperature (°C) Wind speed (m/s) Solar irradiation (W/m$^2$) | Daily | MAPE |
| [56] | Seoul, South Korea | SARIMA | Solar irradiation (MJ/m$^2$) | Hourly Daily Monthly | $R^2$, RMSE |
| Present Study | Hakkâri/Türkiye | ARIMA, SARIMA, HWES, SES | Ambient temperature (°C) Atmospheric pressure (mb) Relative humidity (%) Wind speed (m/s) Solar irradiation (W/m$^2$) | Daily | RMSE, nRMSE, MAPE |

**Table 2** Solar radiation prediction studies conducted in various geographical regions

| Ref. | Study location | Prediction Model | Data Parameters | Time Scale | Performance metrics used |
|---|---|---|---|---|---|
| [57] | Chile | WRF (Weather Research and Forecasting) | Solar irradiance Wind speed Precipitation accumulation | Hourly | MAE |
| [58] | Europe, North Africa | AI satellite retrieval | Satellite SSI Cloud index | Hourly | MBE, RMSE, MAE |
| [59] | Bangladesh | TFT (Transformer, Temporal Fusion Transformer) | Temperature Relative humidity Wind speed and direction Solar irradiation Pressure | Hourly | $R^2$, MSE, MAE |
| [60] | USA | ICEEMDAN, TimesNet | Solar irradiation Temperature Relative humidity Wind speed | Week- Hourly | $R^2$, RMSE, nRMSE, MAE |
| [61] | Japan | CNN LSTM | Solar irradiation Temperature Relative humidity Wind speed | Hourly | $R^2$, RMSE, rRMSE, MSE |

different geographical regions regarding model types, input parameters used, time scales, and performance metrics.

In recent years, data-driven and hybrid methods for solar irradiance forecasting have gained significant attention. To provide a broader geographical scope and to support the comparative assessment of the present study, summary information from several recent international investigations conducted under diverse climatic and meteorological conditions is presented in Table 2.

The use of a daily time scale in this study is significant for evaluating short-term forecasting performance. While

some studies in the literature (e.g., those conducted in Awali, Bahrain, and Seoul, South Korea) rely solely on individual performance metrics such as MAPE or RMSE, this study considers RMSE, nRMSE, and MAPE collectively, offering a more multidimensional assessment of forecasting accuracy. This approach enables a more objective evaluation of model performance. Moreover, whereas many studies utilize only solar irradiation or a limited number of meteorological parameters, the inclusion of atmospheric pressure, an infrequently used but potentially influential variable, constitutes a distinctive contribution of this study. Additionally, conducting the modeling in Hakkâri, a high-altitude region with limited meteorological data infrastructure, provides a valuable reference for areas with similar geographical characteristics.

A review of literature shows that, in solar irradiation prediction studies, which is a very important topic today, various time series models, besides many different DL algorithms, are frequently used. The reason is that solar irradiation is a crucial component of PV systems, and it is necessary to determine it with values close to the actual ones. Additionally, time series methods produce successful results, which have started to be used in all fields today and show superior characteristics compared to existing calculation and prediction methods. However, the rapid change of solar irradiation regionally, seasonally, temporally, and climatically necessitates the preference for Models that include time parameters when selecting solar irradiation prediction models. Accordingly, the contributions of the study can be listed as follows:

- The development of effective time series modelling methods has been a subject of considerable research and development to facilitate more accurate estimation of solar irradiation, a critical parameter in the context of energy production in photovoltaic (PV) systems. Consequently, predictions that will facilitate daily advanced energy production and consumption planning have been provided. This contribution provides a novel application area for the existing literature.
- In the context of time series-based solar irradiation estimation, a combined approach involving hyperparameter optimization (Grid Search) and K-Fold cross-validation methods has been employed. The concurrent utilisation of these two methods is seldom observed in the extant literature. In this respect, an original methodological contribution is presented to the literature.
- In addition to the frequently used ARIMA and SARIMA models that are commonly referenced in the extant literature, the solar irradiation estimation performances of the less frequently studied SES and HWES models have been examined in detail and compared. This contribution augment the extant body of literature by introducing a range of novel methodologies and perspectives.
- The modelling was performed using 5-minute high-resolution meteorological data collected in real time in a region characterised by harsh climate conditions and high seasonal variability, such as Hakkâri province. The corpus of research on time series estimation with this resolution data is relatively limited. By utilising high-resolution data, this study introduces a significant innovation to the existing literature.
- During the data pre-processing stage, low irradiation values in the range of 0–120 W/m², where solar panel production is rendered ineffective, were eliminated from the dataset. Consequently, more meaningful and functional estimates were made using data that would contribute to production. This approach introduces an original data processing technique to the existing literature on the subject.
- A comprehensive evaluation of the performance of different time series models was conducted, utilising a range of error metrics, including RMSE, nRMSE and MAPE, to provide a multifaceted assessment of the models' accuracy and precision. A multi-dimensional analysis was presented, with no reliance on a single performance indicator. This contribution adds methodological richness to model evaluation approaches in the literature.
- Following the implementation of the Grid Search optimisation process, a substantial enhancement was observed in all models, particularly in the Mean Absolute Percentage Error (MAPE) values. This situation demonstrated that hyperparameter optimization can substantially enhance the efficacy of models in time series predictions. This finding provides new evidence that emphasises the importance of hyperparameter optimisation in the relevant literature.
- Recent findings have indicated that in circumstances where high-resolution real meteorological data sets are available, the employment of optimised classical time series methods can yield equivalent, if not superior, results when compared with the utilisation of complex structures such as deep learning. This result provides a critical and original perspective on model selection in the literature.

The rest of the study is organized as follows: Section 2 provides an in-depth overview of the approaches used for solar irradiation prediction. Section 3 details the basic architecture and steps of the prediction models used in this research. Section 4 explains the performance metrics applied and compares the time series models by evaluating their results. The overall findings and discussion are presented in Sect.

5. Section 6 summarizes the study's key insights and offers suggestions for future research in solar irradiation prediction.

## 2 Methodology

Reliable solar irradiation forecasts are essential in photovoltaic energy plants' production planning and grid integration. With these projections, electricity generation can be predicted more accurately, and the balance between energy supply and demand can be managed more effectively. Additionally, the outputs of these models can be utilized in areas such as energy efficiency in buildings, innovative city applications, and the optimization of air conditioning systems. These forecasting models are also an important decision support tool in mapping solar energy potential and conducting feasibility analyses for new solar energy investments. In this context, the models developed can be critical in achieving sustainable development goals based on renewable energy.

Predicting solar irradiation is complex due to its nonlinear nature and high-frequency variations [62]. The primary goal of this study is to develop a highly accurate solar irradiation prediction model using four different time series methods. The following sections offer a detailed introduction to the ARIMA, SARIMA, SES, and HWES methods utilized in the research, along with an explanation of the grid search optimization and the K-Fold Cross-Validation-based restructuring process.

### 2.1 Research Process

This study used data from the meteorological station established in the research area of Hakkâri city center, located in the southeastern part of Türkiye, which has highly suitable areas for PV plant installation along with its neighboring regions. In the study's first phase, solar irradiation prediction models were created using different basic meteorological parameter variables. Additionally, the performance of the prediction models was defined and compared. In the second phase, prediction performances were tested using various time series algorithms. The research process initially involves data set arrangement and preprocessing of the data before model training. Subsequently, to predict and validate solar irradiation, the adjusted meteorological variables are used as input parameters in time series prediction models to obtain the solar irradiation parameter as the model output. Finally, the differences among ARIMA, SARIMA, SES, and HWES models were compared and discussed based on the results obtained from performance indicators.

### 2.2 Data Description and Evaluation

Forecasting solar irradiation using time series models based on key meteorological parameters (such as temperature, humidity, wind speed, cloud cover, etc.) typically focuses on physical environmental variables. However, there are also external factors that indirectly influence this process. Economic trends, government support and resource access may not directly alter meteorological parameters. Still, they can play a decisive role in data quality, the scope of measurement infrastructure and the development of modeling processes. For example, government incentives for renewable energy can lead to an increase in solar energy investments and, consequently, the establishment of more measurement stations, improving the scope and accuracy of the datasets used in modeling. Similarly, during periods of economic downturn, research and infrastructure investments may decrease, negatively affecting the continuity of long-term data and the reliability of models. Additionally, in regions with limited access to resources, the lack of measurement devices can result in data gaps, leading to increased uncertainty in model predictions. Therefore, when developing time series models for solar irradiation forecasting, the indirect effects of external factors should be considered and the role of these factors in data quality and continuity must be taken into account to enhance the accuracy of the models.

In this context, the meteorological data used in this study were collected in real-time at five-minute intervals from a station located at Hakkâri University, which is situated in the city center of Hakkâri, located in the southern part of Türkiye's Eastern Anatolia Region. The area spans 9,521 km² and is at an elevation of 1,755 m, with approximately 14 h of sunlight during certain times of the year and a high solar irradiation potential. The station, part of a small-scale solar energy system (including sensors from Ahlborn used to collect the data), provides a valuable example of Türkiye's unique meteorological conditions due to its location with continental climate characteristics. The data continuously recorded by the station, including atmospheric pressure (mb), ambient temperature (°C), relative humidity (%), wind speed (m/s) and solar irradiation (W/m²), serve as the key parameters used in the modeling process. In this study, in addition to common meteorological parameters such as temperature, humidity, wind speed, and solar radiation, atmospheric pressure was also included as an input variable. The rationale for this inclusion is that variations in atmospheric pressure can indirectly influence the solar radiation reaching the Earth's surface by affecting air masses, cloud formation, and atmospheric stability. The station is supported by government funding and is available for any academic research, with the possibility of intervention if necessary.

Demographic or disciplinary biases are irrelevant since the study relies solely on physical meteorological measurements. However, missing or anomalous values were filtered during the preprocessing step to ensure the reliability and continuity of the data used in the sampling process. Only periods with high data integrity were included in the model. This approach aims to minimize systematic biases that could arise from the station-based sample.

The region where the station is located, Hakkâri province, has a hot and dry climate in summer and a cold climate in winter, making it one of the areas with high potential for solar power plant investments. With government support, several solar energy projects have been planned in this region, and many have already started their operations. The data collected from this area spans from January 2019 to December 2022. Data recorded during equipment malfunctions at the station, particularly during nighttime hours when solar irradiation was not measured, were considered missing data and excluded from the analysis. The forecasting study did not include values measured in the range of 0–120 W/m² for solar irradiation. This is because photovoltaic panels cannot generate sufficient power in the 120 W/m² range. In this context, out of 5.064.450 data points obtained from the station, 1.486.502 were considered missing and excluded from the forecasting process, leaving 3.577.948 data points used in the analysis. The station details and the sample parameter data measured by the sensors at specific time intervals are shown in Fig. 1.

Unwanted data corruptions can occur in data read from a real application set. This dataset should not be used as is because it can lead to incorrect results. Various data preprocessing steps are available to eliminate this issue. In the experiment set used, there are times when the data cannot be processed, meaning there are rows recorded as blank. Instead of filling these missing values with constant values, the linear interpolation method, which can predict new points between two points, is used. Thus, the empty records are filled. In the next step, outlier data is updated with the average of the values. In the final step of data processing, the data is standardized using the min-max normalization method. After the data processing step, the dataset becomes ready for analysis. The processed dataset is subsequently divided into 70% training and 30% testing sets. The ARIMA, SARIMA, SES and HWES time series prediction methods are then applied, with each method being trained on the training set. The error rates of the resulting predictions are assessed using the RMSE, nRMSE and mean absolute percentage error (MAPE) performance evaluation metrics.

## 2.3 Prediction Models

### 2.3.1 ARIMA

The ARIMA approach is a compelling time series prediction tool that integrates three distinct components into a single model. First, the autoregressive (AR) term captures the past real data variability and uses this variability to create the



| Year | Month | Day | Ambient Temp. (°C) | Wind Speed (m/sn) | Relative Hum. (%) | Atmospheric Pres. (hPa) | Solar Rad. (W/m²) |
|---|---|---|---|---|---|---|---|
| 2019 | 03 | 12 | 2,3 | 0,0 | 100 | 812,2 | 2 |
| 2019 | 12 | 30 | -4,9 | 0,1 | 89,1 | 836,4 | 19 |
| 2020 | 06 | 26 | 30,5 | 1,0 | 21,6 | 818,4 | 957 |
| 2020 | 11 | 12 | 23,0 | 3,6 | 92,4 | 828,4 | 9 |
| 2021 | 01 | 19 | -1,0 | 0,3 | 100 | 821,5 | 11 |
| 2022 | 09 | 04 | 21,6 | 1,1 | 34,8 | 812,9 | 467 |



**Fig. 1** Location of Hakkâri, station view and dataset sample

model. Secondly, the integration order, or 'I' term, represents the count of differences applied to achieve stationarity in the time series, addressing any improbable growth patterns in the data. Finally, the moving average (MA) term includes the moving average of previous prediction errors, allowing the model to adjust and correct these errors [63–66].

The ARIMA model is typically represented as ARIMA (p, d, q), where p denotes the order of the AR part, q indicates the order of the MA component and d reflects the level of differencing applied. The general form of the ARIMA (p, d, q) model is as follows [64, 65].

$$\begin{aligned} Z_t &= \sigma_1 Z_{(t-1)} + \sigma_2 Z_{(t-2)} + \cdots \\ &+ \sigma_p Z_{(t-p)} + \delta + a_t - \vartheta_1 a_{(t-1)} \\ &- \vartheta_2 a_{(t-2)} - \ldots - \vartheta_q a_{(t-q)} \end{aligned} \quad (1)$$

In the equation;
$Z_t$ : It represents the estimated time series value.
$\sigma_1, \sigma_2, \ldots, \sigma_p$ : It is the coefficients of the AR part. It indicates the effect of the past values of the series on the current value.
$Z_{t-1}, Z_{t-2}, \ldots, Z_{t-p}$ : It is the time series' past ppp number of lagged (lag) values .
$\delta$ : It represents the constant term (intercept) in the model.
$a_t$ : It represents the current error term (white noise, random error).
$\vartheta_1, \vartheta_2, \ldots, \vartheta_q$ : It is the coefficients of the moving average (MA) part. It defines the effect of the past error terms on the current value.
$a_{t-1}, a_{t-2}, \ldots, a_{t-q}$ : Error terms in previous periods (shocks, disturbances).

As shown in Fig. 2, the ARIMA(p, d,q) model first applies non-seasonal differencing $\Delta^d$ to the raw series $X_t$ to induce stationarity. The transformed series then flows into two parallel components: the AR(p) block produces a linear combination of the past p observations ($\sigma_1 Z_{t-1} + \cdots + \sigma_p Z_{t-p}$). At the same time, the MA(q) block generates a combination of the last q forecast errors ($-\vartheta_1 a_{t-1} - \cdots - \vartheta_q a_{t-q}$). Finally, these two streams (plus any constant term) are summed in the Σ block to yield the forecast $Z_t$. This separation of autoregressive and moving-average elements, bridged by the integration step, underpins ARIMA's ability to model a wide range of stationary time series behaviors.

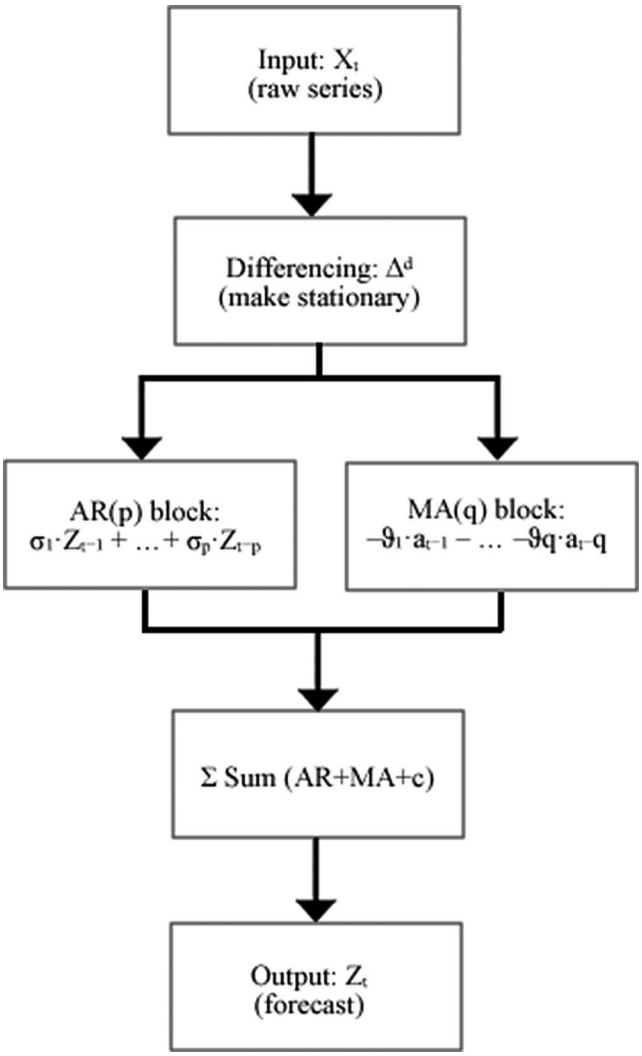



**Fig. 2** Stages of the ARIMA model

### 2.3.2 SARIMA

SARIMA Process: If the series under examination has a monthly or seasonal structure and shows periodic fluctuations in consecutive periods, this indicates the presence of a seasonal effect in the series. If a series is not stationary and contains a seasonal effect, seasonal differencing must be applied to make the series stationary [67–69]. The expression of the SARIMA model is given in Eq. 2 [70].

$$\Phi_p (B^m) \varphi (B) \Delta_S^D \Delta^d X_t = \theta_Q (B^m) \theta (B) w_t \quad (2)$$

In the equation;
$\Phi_p(B^m)$ : Coefficients of the seasonal autoregressive (Seasonal AR) part.
$\varphi(B)$ : Coefficients of the normal AR part.

$\Delta_S^D$ : Seasonal difference operator (to provide seasonal stationarity).
$\Delta^d$ : Normal difference operator (to remove the trend).
$X_t$ : Processed time series value.
$\theta_Q(Bm)$ : Coefficients of the seasonal moving average (Seasonal MA) part.
$\theta(B)$ : Coefficients of the normal moving average (MA) part.
$w_t$ : White noise term (random error).

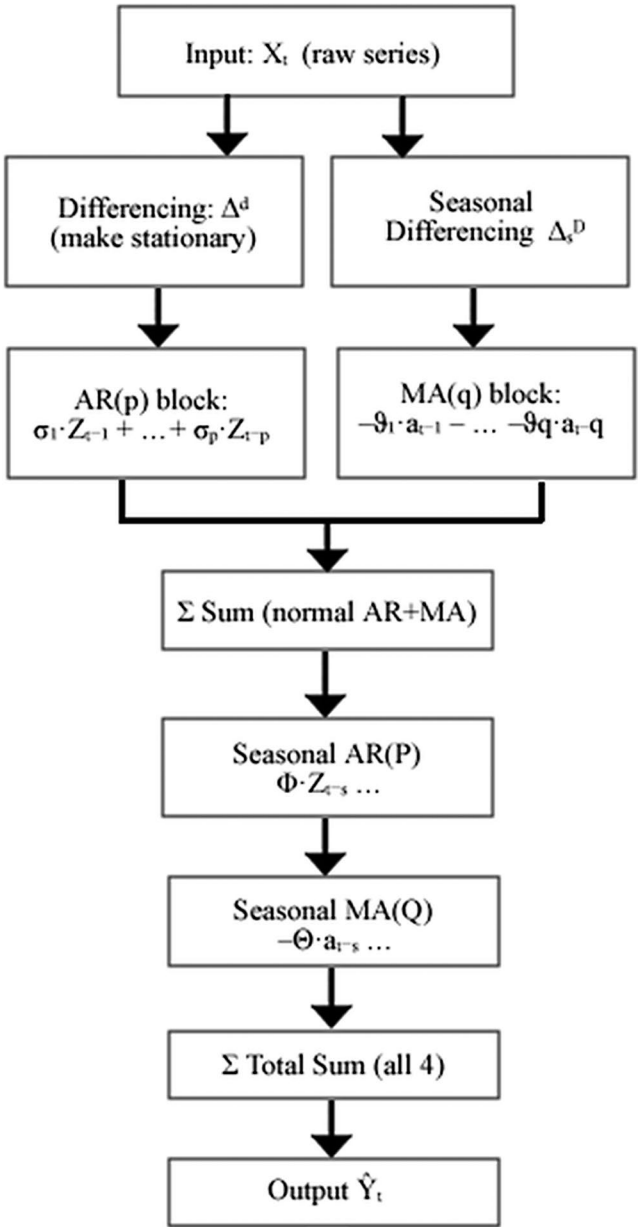



**Fig. 3** Stages of the SARIMA model

Figure 3 extends the ARIMA framework by incorporating seasonal dynamics via additional seasonal differencing $\Delta_S^D$ and seasonal AR and MA components. The raw series $X_t$ undergoes both non-seasonal differencing Δd and seasonal differencing $\Delta_S^D$. The non-seasonally differenced output feeds the AR(p) and MA(q) blocks. In contrast, the seasonally differenced output drives the Seasonal AR(P) and Seasonal MA(Q) blocks at lag sss. All four outputs are merged in the final Σ block to produce the seasonally adjusted forecast $Y^t$ By modeling both short-term fluctuations and recurring seasonal patterns, SARIMA captures complex temporal structures that standard ARIMA cannot.

### 2.3.3 SES

Although this method is helpful and practical with very little computation required, it is not user-friendly. The exponential smoothing model improves prediction by calculating a weighted average of past observations in the time series and gradually reducing the smoothing factor [71–73]. This model is used when there are no cyclical changes or significant trends in the historical data of the dataset. Single, double, and triple exponential smoothing models are widely used [74, 75]. The basic formula for the single exponential smoothing model is provided in Eq. 3 [73].

$$F(t+m) = \alpha y_t + (1-\alpha)\, F_t \tag{3}$$

In the equation;
$F_t$+m : It represents the estimated value at time t+m based on the value at time t.
α : It is the exponential smoothing coefficient (0<α<1). It determines the weight given to past data.
$y_t$ : It is the observed (actual) value at time t.
$F_t$ : It is the estimated value at time t.

Figure 4 illustrates the steps of the SES model. First, the time series data X is taken as input. Next, the appropriate smoothing forecasting model is selected. Based on the chosen model, the initial smoothing value S0 is determined. Using this value and the smoothing coefficient α, the forecast calculation and analysis are performed. Finally, the resulting forecasts are output, allowing the model's performance to be evaluated. This straightforward sequential process provides a fast and effective short- to medium-term prediction when the data exhibit no strong trend or seasonality.

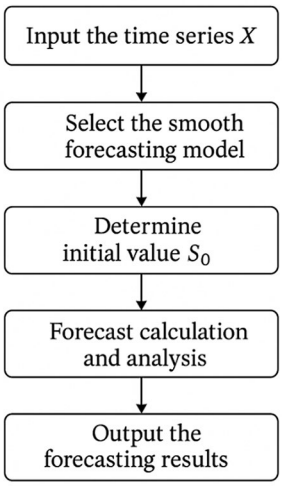



**Fig. 4** Stages of the SES method [76]

### 2.3.4 HWES

The exponential smoothing method assigns decreasing weights to older data points, prioritizing recent observations and thus smoothing the time series. This technique consists of three distinct types. Firstly, single exponential smoothing is well-suited for univariate data that lacks systematic features such as trends or seasonality [77, 78]. Secondly, double exponential smoothing incorporates two parameters, α and β, to adjust for trend variations, handling both additive and multiplicative trends to reduce their impact on future forecasts. Finally, triple exponential smoothing is applied when the time series exhibits seasonality, allowing the model to identify and incorporate seasonal patterns. This technique utilizes three parameters, α, β, and γ, each ranging from zero to one, to manage level, trend, and seasonal components [79].

$$Level: L_t = \alpha(y_t - S_{(t-s)}) + (1-\alpha)(L_{(t-1)} + b_{(t-1)}) \quad (4)$$

In the equation;
$L_t$ : Level component at time t.
α : Correction coefficient used when updating the level ($0<\alpha<1$).
$y_t$ : True observation value.
$S_t$ : Seasonal component (seasonality before sss step).
$L_{t-1}$ : Previous level value.
$b_{t-1}$ : Previous trend value.

$$Trend: b_t = \beta(L_t - L_{(t-1)}) + (1-\beta)\, b_{(t-1)} \quad (5)$$

In the equation;
$b_t$ : Trend component at time t.
β : Correction coefficient used when updating the trend ($0<\beta<1$).
$L_t$ : Current level value.
$L_{t-1}$ : Previous level value.
$b_{t-1}$ : Previous trend value.

$$Seasonality: S_t = y(y_t - L_t) + (1-y)\, S_{(t+m-s)} \quad (6)$$

In the equation;
$S_t$ : Seasonal component at time t.
γ : Correction coefficient that updates seasonality ($0<\gamma<1$).
$y_t$ : Actual observation value.
$L_t$ : Updated level value.
$S_{t-s}$ : Seasonal value s steps ago.

$$Forecast: F_{(t+m)} = L_t + b_t m + S_{(t+m-s)} \quad (7)$$

In the equation;
$F_{t+m}$ : Forecast for t+m steps ahead.
$L_t$ : Current level value.
$b_t$ : Current trend coefficient.
m : Number of steps forward forecast.
$S_{t+m-s}$ : Relevant seasonal component.

The diagram in Fig. 5 depicts the step-by-step procedure for the HWES method. Beginning at "Start" one collects and identifies patterns in the data to capture its level, trend and seasonal behaviors. Next, initial values for the level (L), trend (b) and seasonal (S) components are determined from the first cycle of observations. The smoothing parameters α, β and γ are then selected - typically via grid search or other optimization - to govern how new data update each component. With these in place, the model calculates forecasts by combining the most recent estimates of L, b and S. Finally, the accuracy of the generated forecasts is evaluated using MAE and MAPE before the process terminates at "End" This workflow ensures dynamic adjustment for both trend and seasonality in producing reliable predictions.

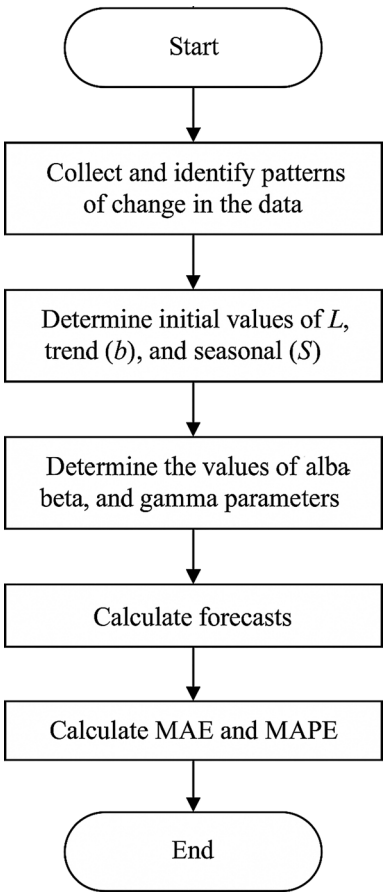



**Fig. 5** Stages of the HWES Method [80]

#### 2.3.5 Grid Search Optimization Algorithm

It is a technique to find the best ML model hyperparameter combinations. In this method, the possible value ranges of the hyperparameters defined by the user are specified and all possible combinations within these ranges are tried to evaluate the model's performance. It evaluates the Cartesian product of a limited set of values the user defines [81]. The model is then trained using each possible combination, and the hyperparameter combination that yields the best performance based on the chosen metric is selected. This process can be computationally intensive due to the exhaustive search it requires, but it is an effective method for achieving optimal results [82].

#### 2.3.6 K-Fold Cross-Validation

This method is employed to assess ML model performance. It entails splitting the dataset into K equal parts, or folds, where each fold serves as a validation set once, while the remaining K-1 folds are utilized for training. This process is repeated K times, with the model being trained and evaluated on each fold sequentially. The average of the validation outcomes from all iterations offers a comprehensive performance estimate for the model [83]. A significant limitation of this approach is that the training algorithm must be run independently for each fold, making the evaluation process K times more time-consuming [84].

#### 2.3.7 Performance Evaluation

In this research, the predicted global solar irradiation generated by four distinct time series algorithms is compared with the actual observed data to evaluate the models' effectiveness. This comparison is essential for assessing the accuracy and reliability of the time series methods used. To quantitatively evaluate the prediction accuracy and identify the optimal model structure, commonly accepted evaluation metrics, including RMSE, nRMSE and MAPE are employed [85–89]. Table 3 provides the corresponding formulas and descriptions for these statistical metrics.

**Table 3** A short overview of the statistical metrics applied in this study

| Metric | Equation |
|---|---|
| RMSE | $RMSE = \sqrt{\frac{1}{N}\sum_{i=1}^{N}(y_i - \widehat{y_i})^2}$ |
| nRMSE | $nRMSE = \frac{\sqrt{\frac{1}{N}\sum_{i=1}^{N}(y_i - \widehat{y_i})^2}}{\bar{y_i}} * 100$ |
| MAPE | $MAPE = \frac{1}{N}\sum_{i=1}^{N}\frac{(y_i - \widehat{y_i})}{y_i} * 100$ |

### 2.4 Model Creations

In this section, the flowchart (Fig. 6) that forms the basis of the study and the general working logic are detailed comprehensively. Additionally, the methodology of the study is clearly presented. The data used in the study were obtained from a specially located meteorological station in Hakkâri between January 2019 and December 2022.

Selecting the parameters used in the models is a very important process. For the ARIMA model, non-seasonal parameters (p, d, q); for the SARIMA model, in addition to the non-seasonal parameters in the ARIMA model, seasonal parameters (P, D, Q, s); for the SES model, the weight adjustment parameter (α); and finally, for the HWES model, in addition to the parameter in the SES model, the trend adjustment parameter (β) are set to obtain the most appropriate values using the Grid Search optimization algorithm. The models are run for prediction using the optimized parameters. Additionally, the acceptability of the results is confirmed by using K-Fold cross-validation in the models. In the models where 5-Fold cross-validation is applied with K = 5, the dataset's each 5 subset is separately used as a test set (with the other 4 subsets as training sets) to obtain the results. In this way, the average of the prediction values obtained as a result of the study is taken, resulting in more acceptable prediction values.

The prediction success rates observed with the standard versions of the models are low. When the appropriate values for the hyperparameters of these models are obtained using the Grid Search optimization algorithm, it is seen that the prediction success increases.

## 3 Result and Discussion

This section presents the detailed comparative studies conducted to evaluate the prediction accuracy and performance of the time series models used for solar irradiation prediction. The input dataset includes variables such as global solar irradiation on the original horizontal plane, temperature, humidity, wind speed and atmospheric pressure. Initially, the time parameters (year, month, day, hour, minute, second) were processed by removing the hour, minute and second data from the station's records. Next, data points where solar irradiation was recorded below 120 W/m² were removed. As a result, the remaining 3.577.948 data points were split into training and test datasets using 5-Fold cross-validation with K = 5.

After the data loading process, the four selected time series prediction models ARIMA, SARIMA, HWES and SES are trained and tested. To measure the performance of

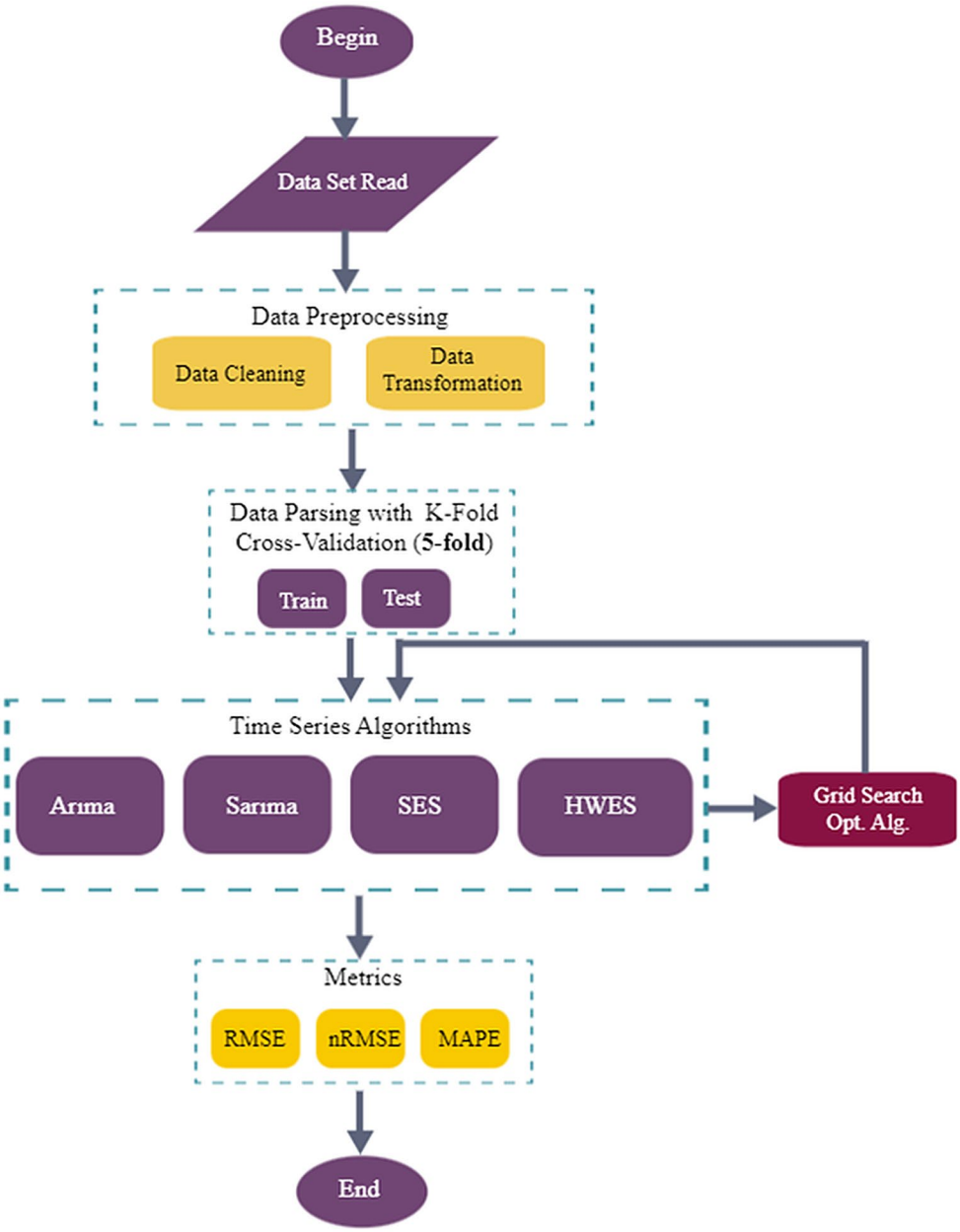



**Fig. 6** Flowchart of the study

the prediction models, RMSE, nRMSE and MAPE error metrics are calculated separately for each model.

## 3.1 Outputs of Prediction Models

### 3.1.1 Outputs of ARIMA

The Arima model's prediction and forecast graph is presented in Fig. 7. It is observed that the ARIMA (3,0,2) model, which yields the optimal result with the grid search optimization algorithm, is successful in capturing the trend. It disregards short-term fluctuations as irrelevant noise and instead focuses on long-term trend changes. It is evident that the model, due to its exclusion of a seasonal term, is incapable of discerning the increases that occur during the summer months. This deficiency in the model is further compounded by a tendency towards correction.

As demonstrated in Fig. 8, the ACF and PACF graphs of monthly total solar irradiation are presented. It is important to note that, given the 0th lag in the PACF graph is always one, it is to be ignored. When the first three lags are examined, the lag 1 and lag 3 bars are above the confidence interval (blue region), while lag 2 remains in the blue region. Consequently, the number of AR terms is determined as $p=3$. Conversely, within the ACF graph, the 0th lag is disregarded, and two consecutive bars in lag 1 and lag 2 exhibit a robust correlation above the confidence interval. In subsequent lags, the correlation swiftly reverts to the blue region.

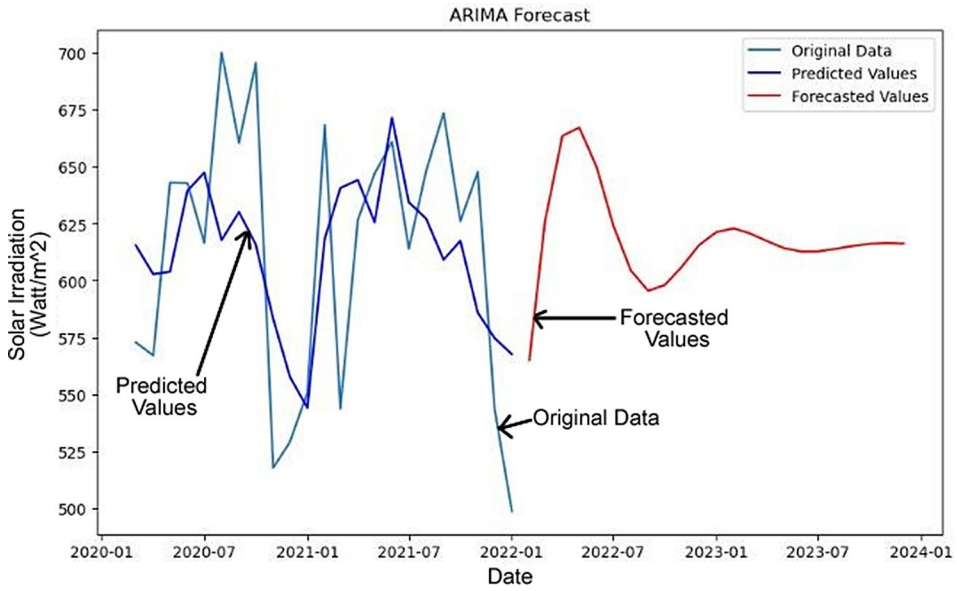



**Fig. 7** Prediction and forecast results of ARIMA

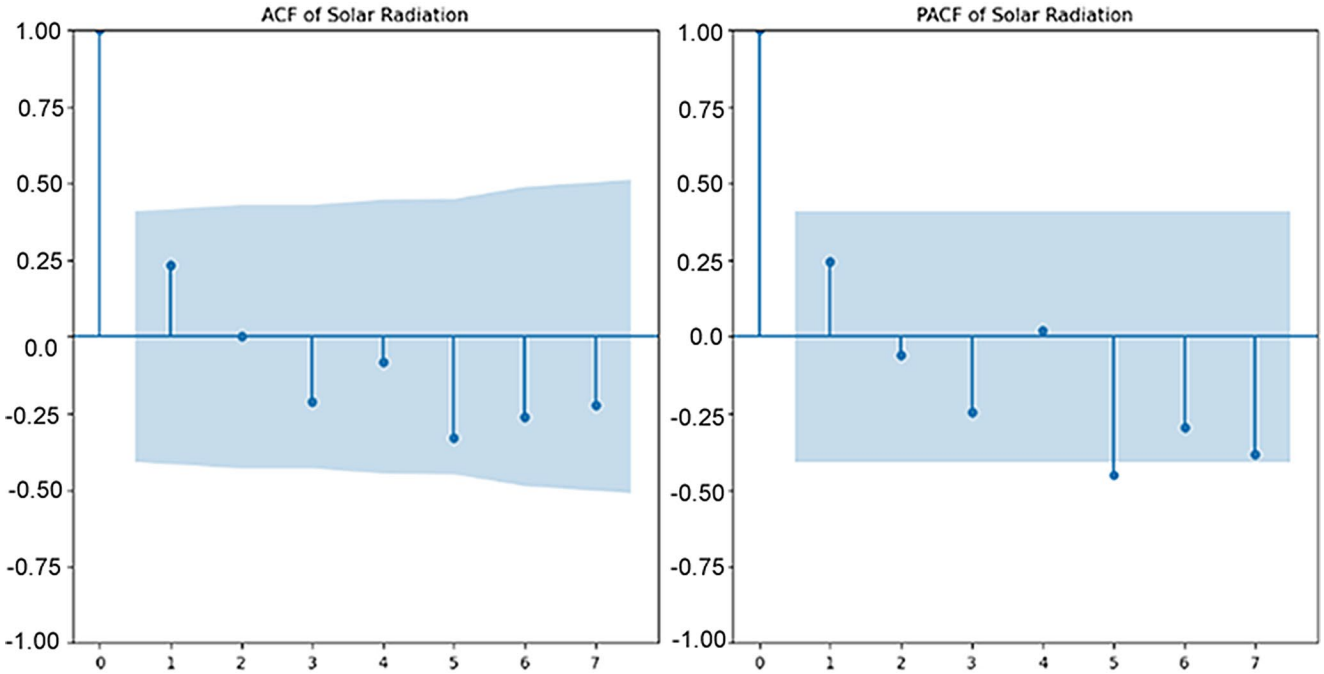



**Fig. 8** ACF and PACF plots for ARIMA

Consequently, the number of MA terms should be q=2. It is evident that, in the absence of any supplementary differencing operations being applied to the series, the d value is equivalent to 0.

As illustrated in Fig. 9, the graphical diagnostics are presented. In the time series of the residuals (Fig. 9 (a)), random fluctuations are observed around the zero mean. There is no significant seasonality. It can be posited that the model exhibits a predominantly constant variance. When the histogram of the residuals is examined (see Fig. 9 (b)), a distribution close to a symmetrical structure focused on the zero point is evident. Despite slightly elevated values that give rise to a slight tail in the distribution curve, it can be posited that the data is, in all probability, proximate to a normal distribution. As illustrated in Fig. 9 (c) of the Normal Q-Q graph of the residuals, the data points are observed to be concentrated around or near the reference line. Given that the deviations of the extreme points are also near the reference line, it can be deduced that a normal distribution closely approximates the distribution. In the ACF graph of the residuals (see Fig. 9 (d)), except for lags 1–3, all points (correlation coefficients) are contained within the blue

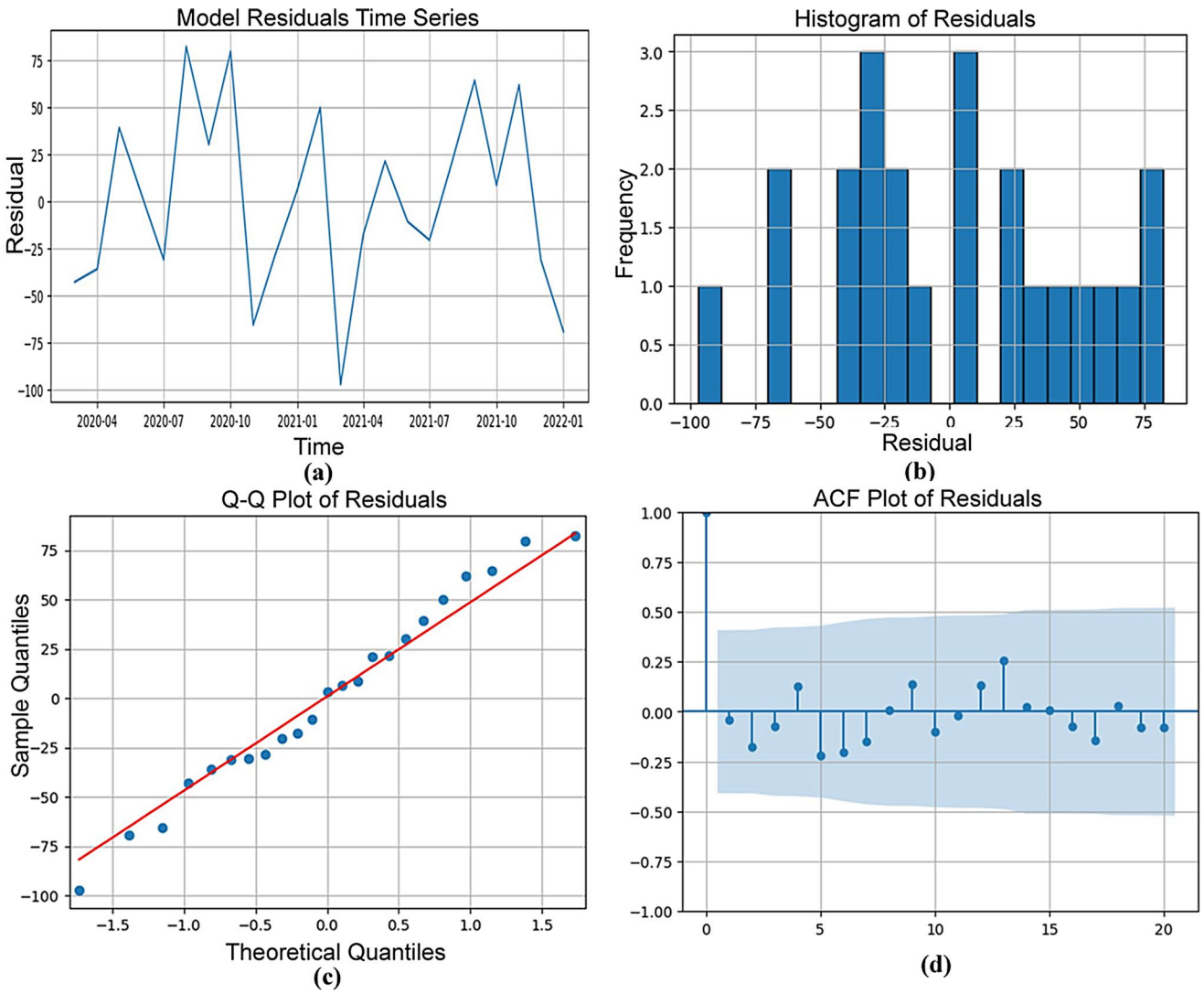



**Fig. 9** Plot diagnostics of ARIMA

confidence interval. In summary, the variable is devoid of substantial autocorrelation.

The findings indicate that the ARIMA (3,0,2) model possesses adequate calibration properties (zero mean, constant variance, normal distribution and autocorrelated residuals) for this particular data set, ensuring its reliability.

### 3.1.2 Outputs of SARIMA

As illustrated in Fig. 10, the prediction and forecast graph of the SARIMA model is presented. It is observed that the SARIMA (2,0,2) (1,0,1,12) model, which yields the optimal result with the grid search optimization algorithm, is successful in capturing the trend and seasonal terms. The data demonstrate a satisfactory correlation between high and low values during summer and winter, respectively. These seasonal fluctuations enrich the predictions. Incorporating a seasonal term within the model facilitates the generation of more realistic long-term predictions in solar irradiation data.

As demonstrated in Fig. 11, the ACF and PACF graphs of monthly total solar irradiation are presented. It is important to note that, given the 0th lag in the PACF graph is always equal to 1, this is ignored. Upon examination of the successive lags, a substantial positive deviation is observed in lag 1, a value within the blue region in lag 2, and a minor external deviation in lag 5. This pattern indicates that the number of non-seasonal AR terms (p) is 2. In the ACF graph, except for lag 0, two bars in lag 1 and lag 2 demonstrate a strong positive correlation above the confidence interval. This correlation rapidly reverts to the blue region in the subsequent lags. Therefore, the number of non-seasonal MA terms (q) is selected as 2. Since there is a relatively weak but consistent bar output in the ACF and PACF at the 12th lag at the seasonal level (s = 12), the seasonal AR and MA term numbers

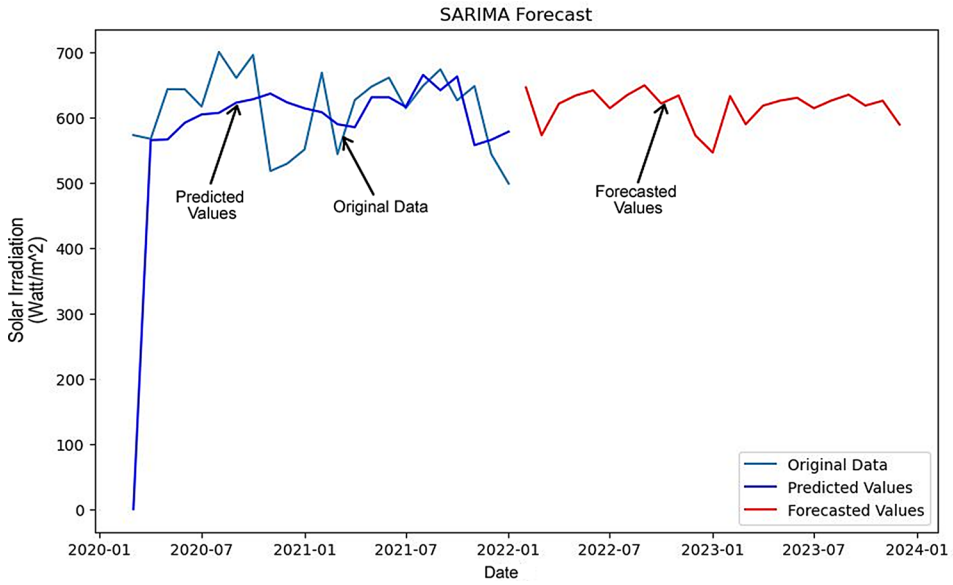



**Fig. 10** Prediction and forecast results of SARIMA

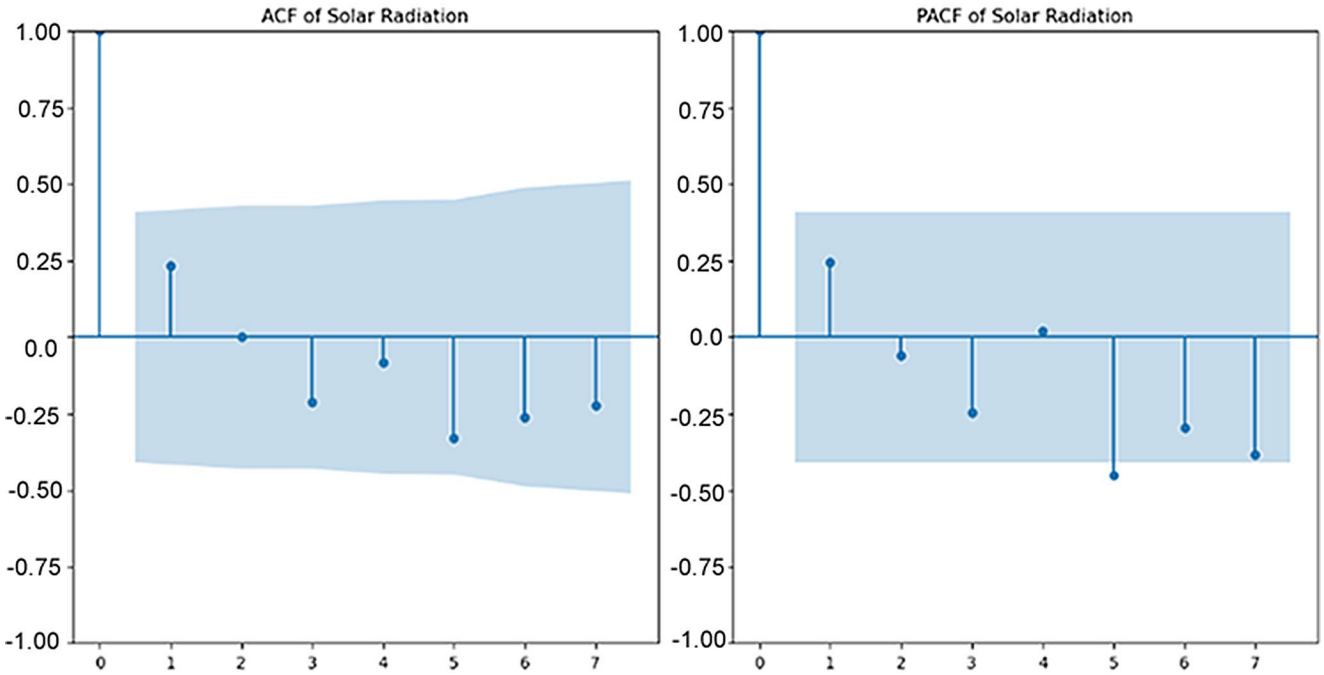



**Fig. 11** ACF and PACF plots for SARIMA

are determined as $P=1$ and $Q=1$, respectively. Without any additional difference (d and D) being applied to the series, both values are 0.

Consequently, the SARIMA (2,0,2)(1,0,1,12) model, which utilises both short-term ($P=2$, $Q=2$) and seasonal ($P=1$, $Q=1$, $S=12$) parameters, provides a consistent explanation for these correlation patterns.

The graphical diagnostics are displayed in Fig. 12. As illustrated in Fig. 12 (a), the time series of the residuals exhibits random fluctuations around a zero mean. There is no significant rising or falling trend and no regular seasonality. It can be posited that the model exhibits a predominantly constant variance. As illustrated in Fig. 12 (b), the residuals' histogram demonstrates a distribution closely aligned with a symmetrical configuration, with a pronounced concentration around the zero point. While one or two extreme points give rise to slightly thick tails, it can be posited that the distribution approaches a normal one. As illustrated in Fig. 12 (c), the Normal Q-Q graph of the residuals demonstrates that the data points are situated above or near the reference line. The deviations of the high and low extreme points are also close to the reference line, indicating that the

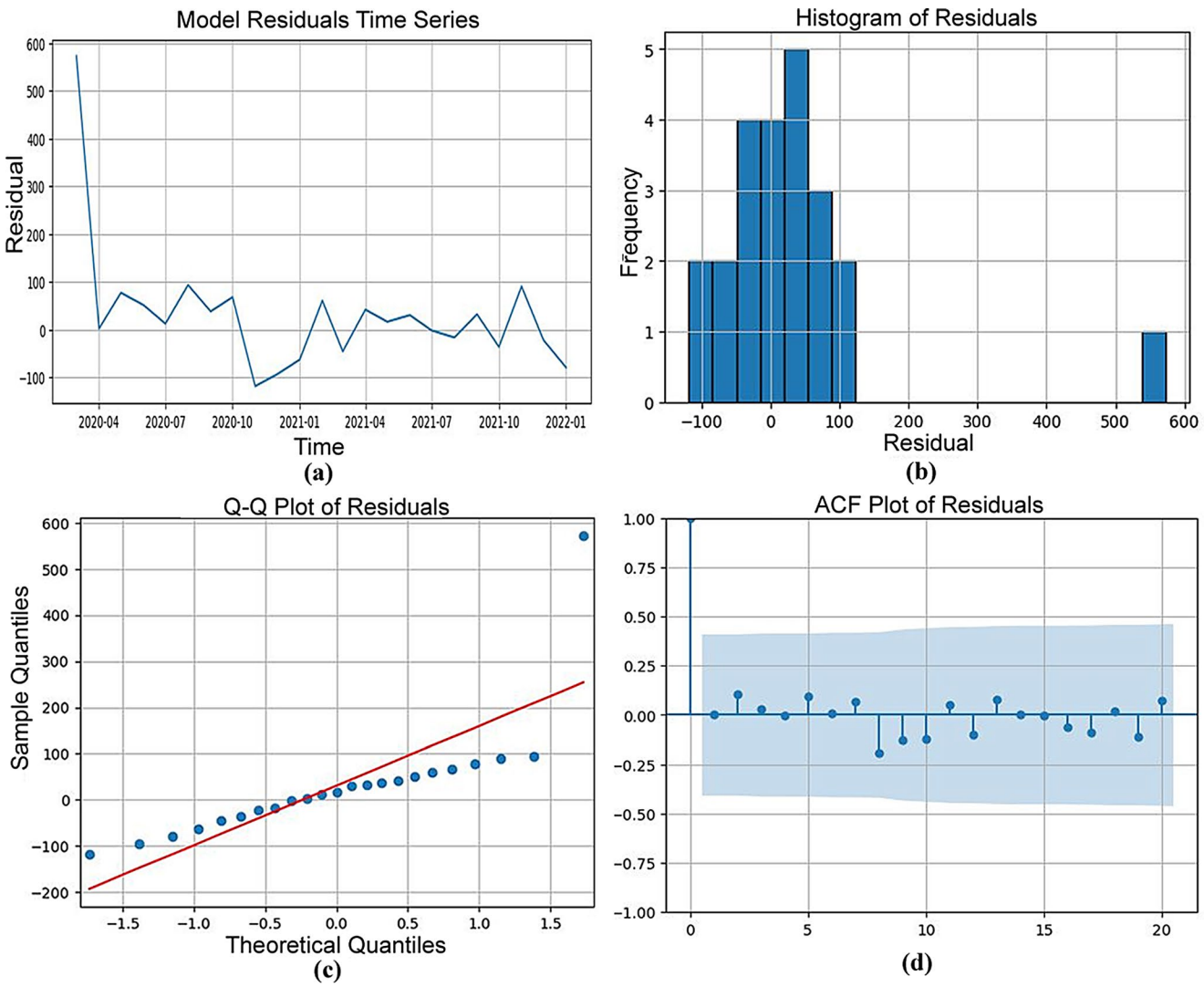



**Fig. 12** Plot diagnostics of SARIMA

distribution is close to a normal distribution. As illustrated in Fig. 12 (d), the ACF graph of the residuals demonstrates that all lags 1–20 are contained within the blue confidence interval. In summary, the variable is devoid of substantial autocorrelation. There is a presence of minute positive bars, which are located far below the significant limit. These bars are only observed around lag1 and lag9.

The results reveal that the SARIMA(2,0,2)(1,0,1,12) model has suitable calibration properties for this data set and can be used reliably.

### 3.1.3 Outputs of HWES

Figure 13 shows the HWES model's prediction and forecast graph. It follows the short-term average by making an elementary-level correction. Since it cannot model seasonal ups and downs, it cannot predict summer-winter differences.

As demonstrated in Fig. 14, the ACF and PACF graphs of monthly total solar irradiation are presented. In the context of ACF, the exclusion of lag 0 reveals a notable positive correlation (approximately + 0.25) that surpasses the confidence interval (demarcated by the blue region). Weak negative deviations are observed in the 3rd, 5th, 6th and 7th lags immediately following it. It has been demonstrated that, at elevated lags, the correlation rapidly reverts to the confidence region. This finding indicates that the series exhibits short-term memory, yet the autocorrelation diminishes significantly over time. In the PACF, lag 1 is particularly noteworthy with an approximate value of + 0.25. A.

minor negative value is evident in lag 2, with a substantial deviation of approximately − 0.25 in lag 3 and − 0.45 in lag 5. It is noteworthy that the PACF bars persist within the confidence interval. The aforementioned patterns indicate the suitability of the HWES method for data devoid of

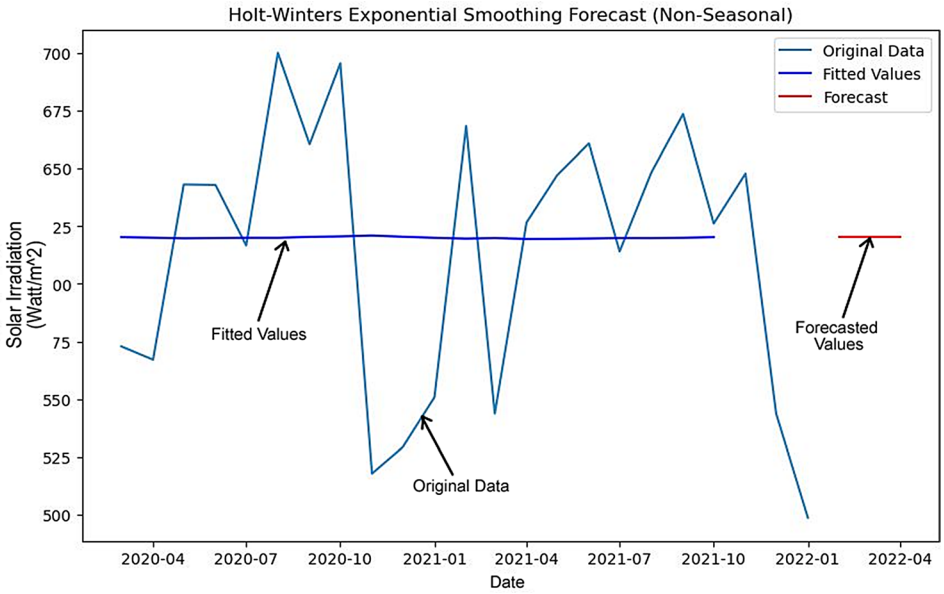



**Fig. 13** Prediction and forecast results of HWES

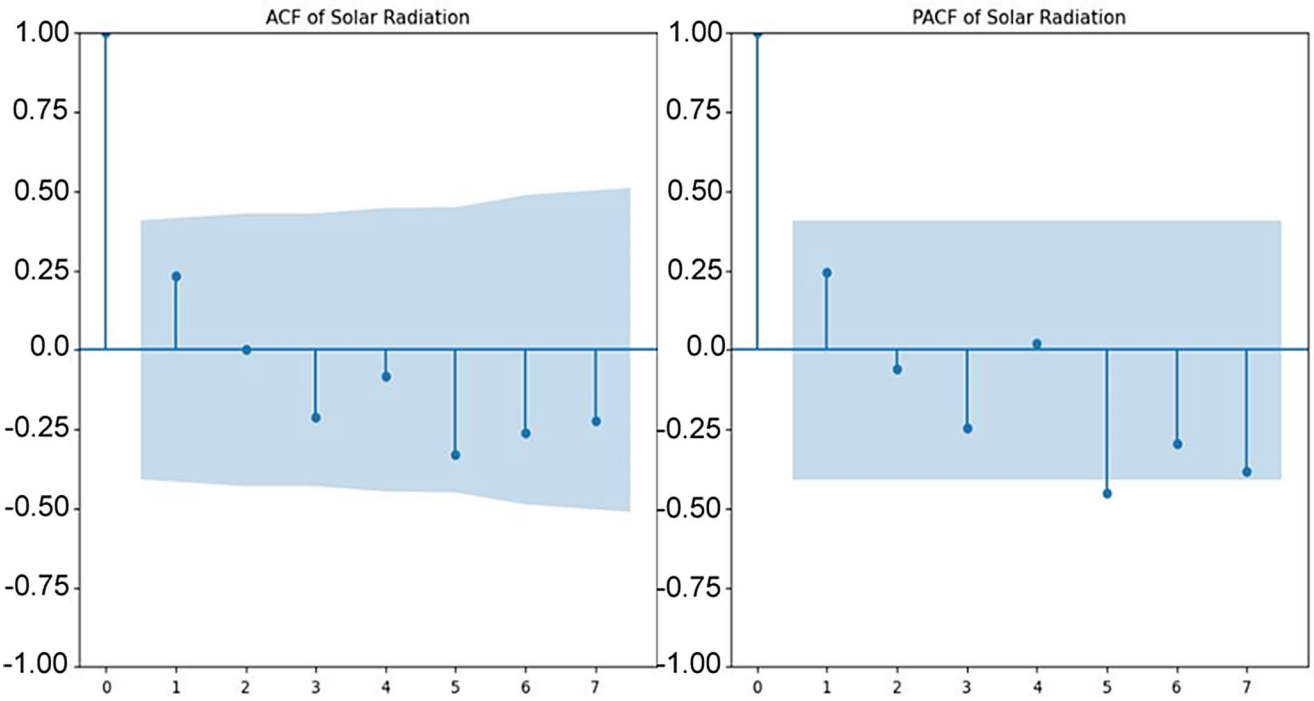



**Fig. 14** ACF and PACF plots for HWES

seasonal elements, yet exhibiting a slightly persistent trend and short-term dependence. The created model structure successfully captures the lag 1 effect with a single smoothing parameter (α) and stabilises the series in the long term.

As demonstrated in Fig. 15, the graphical diagnostics reveal random fluctuations around the zero mean in the time series of the residuals (see Fig. 15 (a)). There is no significant rising or falling trend and no regular seasonality. It can be posited that the model exhibits a predominantly constant variance. As illustrated in Fig. 15 (b), the residuals' histogram demonstrates a distribution close to a symmetrical structure, with a concentration around the zero point. While the presence of extreme points gives rise to slightly thick tails, it can be posited that the distribution approaches a normal curve. As illustrated in Fig. 15 (c), the Normal Q-Q graph of the residuals demonstrates that the data points are closely aligned with the reference line. The deviations of the high and low extreme points are also close to the reference line, indicating that the distribution is close to a normal distribution. As illustrated in Fig. 15 (d), the ACF graph of

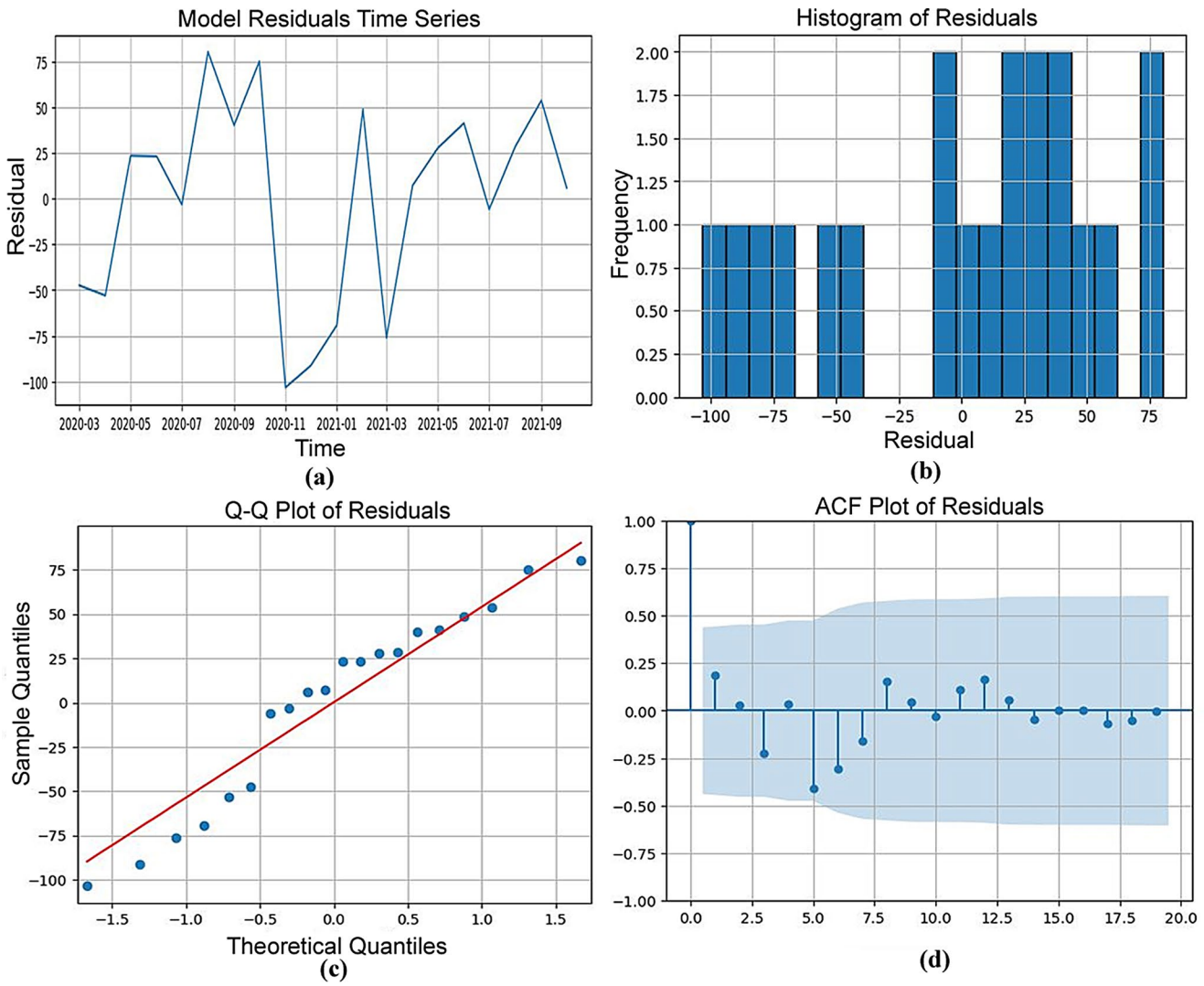



**Fig. 15** Plot Diagnostics of HWES

the residuals demonstrates that all lags 1–20 are contained within the blue confidence interval. In summary, the evidence indicates that there is no significant autocorrelation residue.

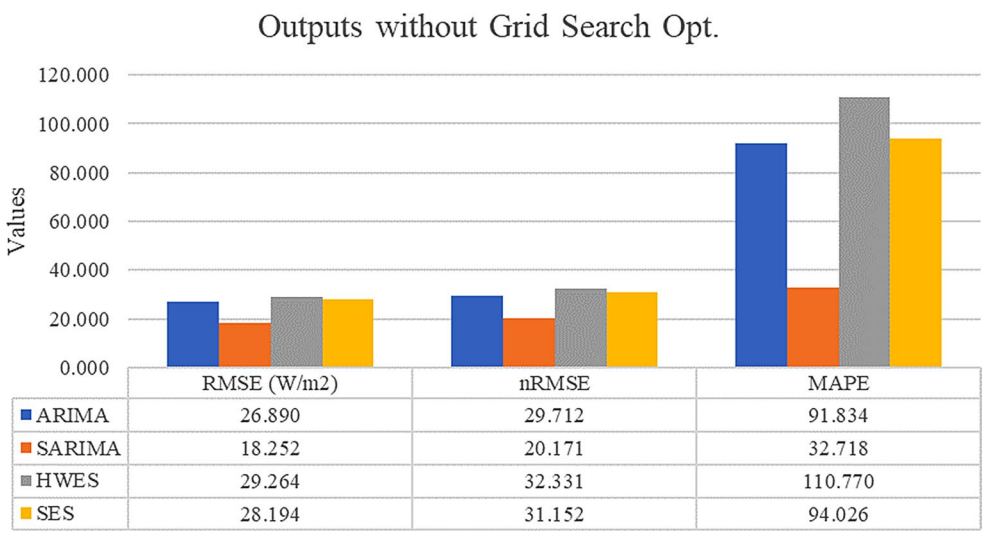
The findings indicate that the HWES model, utilising solely the level (α) parameter without trend (β) and seasonality (γ), exhibits adequate calibration properties for this data set and can be relied upon. It is important to note that the grid-search optimisation method employed for the HWES model indicates that among the.

#### 3.1.4 Outputs of SES

It has been observed that the grid search optimisation method applied to the HWES model is the model with the lowest error and no trend or seasonality. It has been demonstrated that this method is mathematically equivalent to the SES method, and all results obtained are equal. Consequently, the graphs and explanations of the SES method are not reiterated.

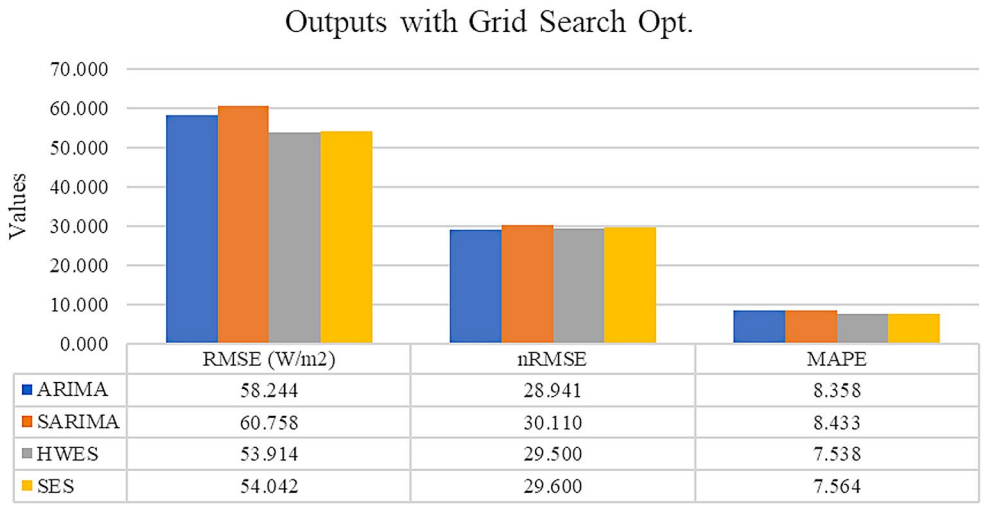
### 3.2 Comparison of Prediction Models

Statistical error metrics were calculated to analyze how much the model results deviated from the observed data. Figures 16 and 17 show the results obtained from the performance measurements of different models used in the study. Among the time series models, the SARIMA model demonstrates the best performance with RMSE and nRMSE values of 18.252 W/m² and 20.171%, respectively, before optimization. The results obtained with the ARIMA model are also satisfactory. The HWES and SES models exhibit the worst performance with the highest RMSE and MAPE values. This indicates that the SARIMA model is more effective for time series data, while the HWES and SES models are weak in prediction accuracy.




| | RMSE (W/m2) | nRMSE | MAPE |
|---|---|---|---|
| ARIMA | 26.890 | 29.712 | 91.834 |
| SARIMA | 18.252 | 20.171 | 32.718 |
| HWES | 29.264 | 32.331 | 110.770 |
| SES | 28.194 | 31.152 | 94.026 |

**Fig. 16** Outputs without grid search opt




| | RMSE (W/m2) | nRMSE | MAPE |
|---|---|---|---|
| ARIMA | 58.244 | 28.941 | 8.358 |
| SARIMA | 60.758 | 30.110 | 8.433 |
| HWES | 53.914 | 29.500 | 7.538 |
| SES | 54.042 | 29.600 | 7.564 |

**Fig. 17** Outputs with grid search opt

After Grid Search optimization, a general decrease in RMSE and nRMSE values was observed for all models, but there was a significant reduction in MAPE values. Specifically, the MAPE for the ARIMA model dropped from 91.834% to 8.358% and for the SARIMA model, it decreased from 32.718% to 8.433%. This demonstrates that optimization improves the precision of predictions and helps the models make more accurate predict. Therefore, it can be said that among the four different time series models used in the study, the SARIMA model is successful and usable for predicting global solar irradiation on a horizontal plane. The success graphs comparing the actual solar irradiation values with the prediction data obtained from all-time series models are shown in Fig. 17.

Without optimization, the SARIMA model exhibits the best performance. However, with Grid Search optimization, a significant improvement in MAPE values has been achieved, increasing the prediction accuracy of the models. This indicates three alternatives ("add", "mul", "None"), the trend=None (i.e. only level correction) option yields the optimal error (MSE). It has been demonstrated that this scenario is mathematically equivalent to SES, thereby ensuring that the HWES outcomes are congruent with the SES results that optimization effectively enhances the overall accuracy of the models. It is important to consider both RMSE and MAPE values in model selection, balancing performance metrics. Optimization can improve specific metrics while potentially negatively affecting others, so maintaining this balance during the model evaluation process plays a critical role. Table 4 shows the performance evaluation results of the prediction methods with and without optimization applied to solar irradiation prediction success.

As shown in Table 4, the SARIMA model is effective for accurately predicting the monthly average global solar irradiation on a horizontal plane. The RMSE, nRMSE and MAPE values for the SARIMA model fall within acceptable limits compared to other models. Consequently, among the four time series models evaluated in this study, the SARIMA model is the most reliable for predicting global solar irradiation. The graphs illustrating the performance of the time

**Table 4** Performance evaluation results of prediction methods with and without optimization

| Model | Outputs before using Grid Search Opt. | | | Outputs using Grid Search Opt. | | |
|---|---|---|---|---|---|---|
| | RMSE (W/m$^2$) | nRMSE (%) | MAPE (%) | RMSE (W/m$^2$) | nRMSE (%) | MAPE (%) |
| ARIMA | 26.890 | 29.712 | 91.834 | 58.244 | 28.941 | 8.358 |
| SARIMA | 18.252 | 20.171 | 32.718 | 60.758 | 30.110 | 8.433 |
| HWES | 29.264 | 32.331 | 110.770 | 53.914 | 29.500 | 7.538 |
| SES | 28.194 | 31.152 | 94.026 | 54.042 | 29.600 | 7.564 |

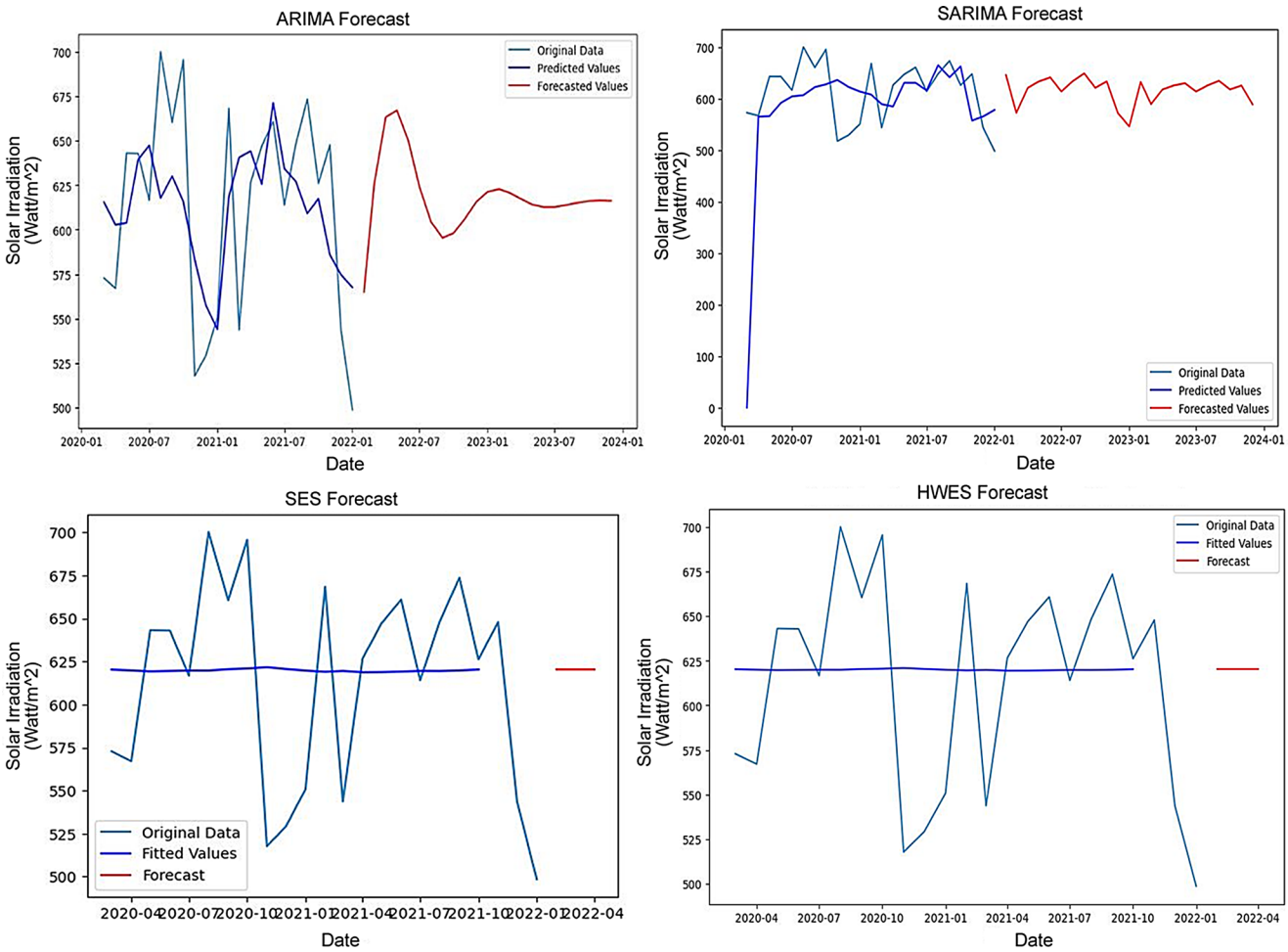



**Fig. 18** Comparison of the actual solar irradiation values with the predicted data obtained from all-time series models

series methods used in predicting global solar irradiation on a horizontal plane are displayed in Fig. 18.

According to Fig. 18, the SARIMA model appears to be the best fit for the original data. This model makes predictions by considering both trend and seasonal components, and its forward predictions seem more accurate than other models. The ARIMA model also shows reasonable performance but slightly more deviation than the SARIMA model. Although the HWES and SES models show more suitable results according to the performance indicators in Table 4, their trends in the graphical results in Fig. 18 are not as smooth. This indicates that the ARIMA and SARIMA models exhibit more stable prediction performance than the HWES and SES models and work more harmoniously with the optimization method.

### 3.3 Evaluation of the Findings in the Context of the Literature and Limitations

This study has proven that the SARIMA model, optimised using grid search, provides a reliable baseline model for solar radiation forecasting in the Hakkâri region (see Table 4 for optimized MAPE of 8.433%). Our findings demonstrate that classical time series models can deliver strong performance, particularly for univariate series, when hyperparameters are carefully optimised.

However, when considered alongside recent methodological advances, particularly those focusing on deep learning and hybrid models, it is evident that the field of research has evolved significantly.

Methodological comparison and strengths:

The main strength of our study is its alignment with recent studies that emphasise the importance of forecasting for practical systems. Examples of these studies include the use of two-stage power forecasting for maximum power point tracking (MPPT) control [48] and the application of distributed model predictive control (DMPC) for energy storage (ES) planning [45]. Establishing a reliable SARIMA baseline is a critical first step for such advanced control and optimisation systems. For instance, the power estimation required by an improved P&O algorithm can be achieved using a statistical method, as demonstrated in our study.

Limitations and a Bridge to Future Work:

- The study's main limitation - which also holds the most significant potential for future work - is that the classical model (SARIMA) used focuses primarily on past data values (autocorrelation). However, recent literature has shifted towards deep learning and hybrid models [37–39].
- Spatio-Temporal Dependencies: Graph neural networks are used to model clusters of power plants rather than single points. Examples of this approach include AHSTGNN for wind forecasting [37] and STDGAT-BILSTM for PV forecasting [38]. These models can learn complex dynamic relationships between stations, such as the "spatial convergence effect" (SFACED) [38]. However, our approach, which focuses on a single region (Hakkâri), is unable to capture such spatial dependencies. Future studies could test GNN-based models using data from multiple stations in Hakkâri and the surrounding area.
- Nonlinear Feature Extraction: Approaches such as CNN-LSTM hybrid models and a specialised feature extraction (EIIR) algorithm have been used to capture peaks and troughs in load forecasting [39]. Solar radiation data can also exhibit sudden changes (e.g. cloud cover). The difficulties that SARIMA encounters when modelling such nonlinear sudden changes can be overcome by using hybrid deep learning architectures [39].
- Integration of Optimization and Decision Making: This study focuses on forecasting. However, the integration of these predictions into decision-making processes is also demonstrated in the current literatüre [43–45]. For instance, the Genetic Algorithm has been employed to optimise the capacity of a multi-energy power plant [43], while two-layer optimisation frameworks such as Robust IGDT have been suggested for economic planning in the face of uncertainty [45]. Our prediction model could potentially serve as input data for such optimisation models in the future. This could include the integration of a PV plant to be built in Hakkâri with innovative systems, such as a PV-Trombe wall, or thermodynamic analyses of the system.

In conclusion, while our study demonstrates the performance of classical models optimised for a local region, the literature proposed in this study provides a clear roadmap for further improving prediction accuracy and translating these predictions into practical engineering decisions.

## 4 Conclusion

This study examined time series-based models for predicting solar irradiation, an important parameter affecting the power generation of PV systems, based on different meteorological parameters. In this context, the applicability and validity of ARIMA, SARIMA, SES and HWES models for predicting global solar irradiation on a horizontal plane were comprehensively evaluated using real meteorological data from Hakkâri province. According to the evaluations, the SARIMA model demonstrated superior performance among the time series models, based on graphical results (Figs. 17 and 18) and general performance evaluation criteria (Table 4). Especially with grid search optimization, more successful prediction results were obtained. In this context, the MAPE value, calculated as 32.718 before optimization, was reduced to 8.433 after optimization. Additionally, RMSE and nRMSE results were within reasonable limits. The ARIMA, HWES and SES models also exhibited performance similar to the results obtained with the SARIMA model in solar irradiation prediction. Particularly when evaluated based on the MAPE performance indicator, significant improvement was achieved after applying optimization in all four models, especially the HWES model. However, the HWES and SES models did not confirm this based on the graphical results. Nevertheless, it was confirmed that applying optimization to the time series models used in this study leads to more successful results in solar irradiation prediction.

Overall, it was determined that the proposed models showed good performance and successful results in solar irradiation prediction studies. Accordingly, it is beneficial to use these models in different climate regions, especially in areas where other climate variables, besides the

meteorological parameters used in the study, are absent. In this context, the study's findings can be used by engineers and researchers to improve the modeling and planning of solar energy systems. For future research, the most successful prediction model based on time series predicting methods can be used to manage renewable energy sources more efficiently and effectively.

**Acknowledgements** This study was not supported by any organization.

**Author Contribution** All authors equally contributed to the study conception and design, data preprocessing, model development, analysis and interpretation of results, and manuscript drafting and revision.

**Funding** No external funding was received for this work.

**Data Availability** The datasets generated and/or analyzed during the current study are available from the corresponding author upon reasonable request and subject to permission from the data provider.

## Declarations

**Competing Interests** Faruk Ayata, Ebubekir Seyyarer and Erşan Ömer Yüzer declare that we have no competing financial interests or personal relationships that could have appeared to influence the work reported in this paper.

## References

1. Gürel AE, Ağbulut Ü, Biçen Y (2020) Assessment of machine learning, time series, response surface methodology and empirical models in prediction of global solar radiation. J Clean Prod 277:122353
2. Ağbulut Ü, Gürel AE, Biçen Y (2021) Prediction of daily global solar radiation using different machine learning algorithms: evaluation and comparison. Renew Sustain Energy Rev 135:110114
3. Besharat F, Dehghan AA, Faghih AR (2013) Empirical models for estimating global solar radiation: a review and case study. Renew Sustain Energy Rev 21:798–821
4. Bailek N, Bouchouicha K, Al-Mostafa Z, El-Shimy M, Aoun N, Slimani A, Al-Shehri S (2018) A new empirical model for forecasting the diffuse solar radiation over Sahara in the Algerian big South. Renewable Energy 117:530–537
5. Fan J, Chen B, Wu L, Zhang F, Lu X, Xiang Y (2018) Evaluation and development of temperature-based empirical models for estimating daily global solar radiation in humid regions. Energy 144:903–914
6. Feng Y, Gong D, Jiang S, Zhao L, Cui N (2020) National-scale development and calibration of empirical models for predicting daily global solar radiation in China. Energy Conv Manag 203:112236
7. Wattan R, Masiri I, Buntoung S, Phoemwong C, Janjai S (2023) An empirical model for estimating the monthly average daily global solar radiation from ground-and satellite-based meteorological data. J Renew Energy Smart Grid Technol 18(1):29–35
8. Mohammadi B, Moazenzadeh R, Pham QB, Al-Ansari N, Rahman KU, Anh DT, Duan Z (2022) Application of ERA-Interim, empirical models and an artificial intelligence-based model for estimating daily solar radiation. Ain Shams Eng J 13(1):101498
9. Fan J, Wang X, Wu L, Zhang F, Bai H, Lu X, Xiang Y (2018) New combined models for estimating daily global solar radiation based on sunshine duration in humid regions: A case study in South China. Energy Conv Manag 156:618–625
10. Bhatt A, Ongsakul W, Singh JG (2022) Sliding window approach with first-order differencing for very short-term solar irradiance forecasting using deep learning models. Sustain Energy Technol Assess 50:101864
11. Liu Y, Zhou Y, Chen Y, Wang D, Wang Y, Zhu Y (2020) Comparison of support vector machine and copula-based nonlinear quantile regression for estimating the daily diffuse solar radiation: A case study in China. Renewable Energy 146:1101–1112
12. Hissou H, Benkirane S, Guezzaz A, Azrour M, Beni-Hssane A (2023) A novel machine learning approach for solar radiation Estimation. Sustainability 15(13):10609
13. Alzahrani A, Shamsi P, Dagli C, Ferdowsi M (2017) Solar irradiance forecasting using deep neural networks. Procedia Comput Sci 114:304–313
14. Reikard G (2009) Predicting solar radiation at high resolutions: A comparison of time series forecasts. Sol Energy 83(3):342–349
15. Paoli C, Voyant C, Muselli M, Nivet ML (2010) Forecasting of preprocessed daily solar radiation time series using neural networks. Sol Energy 84(12):2146–2160
16. Yang D, Jirutitijaroen P, Walsh WM (2012) Hourly solar irradiance time series forecasting using cloud cover index. Sol Energy 86(12):3531–3543
17. Belmahdi B, Louzazni M, Bouardi E, A (2020) One month-ahead forecasting of mean daily global solar radiation using time series models. Optik 219:165207
18. Chodakowska E, Nazarko J, Nazarko Ł, Rabayah HS, Abendeh RM, Alawneh R (2023) Arima models in solar radiation forecasting in different geographic locations. Energies 16(13):5029
19. Boualit SB, Mellit A (2016 November) SARIMA-SVM hybrid model for the prediction of daily global solar radiation time series. In 2016 International Renewable and Sustainable Energy Conference (IRSEC) (pp. 712–717). IEEE
20. Alsharif MH, Younes MK, Kim J (2019) Time series ARIMA model for prediction of daily and monthly average global solar radiation: the case study of Seoul, South Korea. Symmetry 11(2):240
21. Kardakos EG, Alexiadis MC, Vagropoulos SI, Simoglou CK, Biskas PN, Bakirtzis AG (2013 September) Application of time series and artificial neural network models in short-term forecasting of PV power generation. In 2013 48th International Universities' Power Engineering Conference (UPEC) (pp. 1–6). IEEE
22. Bouzerdoum M, Mellit A, Pavan AM (2013) A hybrid model (SARIMA–SVM) for short-term power forecasting of a small-scale grid-connected photovoltaic plant. Sol Energy 98:226–235
23. Dong Z, Yang D, Reindl T, Walsh WM (2013) Short-term solar irradiance forecasting using exponential smoothing state space model. Energy 55:1104–1113
24. Deng C, Zhang X, Huang Y, Bao Y (2021) Equipping seasonal exponential smoothing models with particle swarm optimization algorithm for electricity consumption forecasting. Energies 14(13):4036
25. Cadenas E, Jaramillo OA, Rivera W (2010) Analysis and forecasting of wind velocity in chetumal, Quintana roo, using the single exponential smoothing method. Renewable Energy 35(5):925–930
26. Wu J, Chan CK (2013) Prediction of hourly solar radiation with multi-model framework. Energy Conv Manag 76:347–355
27. Pacurar A, Stefu N, Mares O, Paulescu E, Calinoiu D, Pop N, Paulescu M (2013) Forecasting hourly global solar irradiation using simple non-seasonal models. J Renew Sustain Energy, 5(6)
28. Azimi R, Ghayekhloo M, Ghofrani M (2016) A hybrid method based on a new clustering technique and multilayer perceptron

neural networks for hourly solar radiation forecasting. Energy Conv Manag 118:331–344
29. Trapero JR, Kourentzes N, Martin A (2015) Short-term solar irradiation forecasting based on dynamic harmonic regression. Energy 84:289–295
30. Almazrouee AI, Almeshal AM, Almutairi AS, Alenezi MR, Alhajeri SN, Alshammari FM (2020) Forecasting of electrical generation using prophet and multiple seasonality of holt–winters models: A case study of Kuwait. Appl Sci 10(23):8412
31. Jiang W, Wu X, Gong Y, Yu W, Zhong X (2020) Holt–Winters smoothing enhanced by fruit fly optimization algorithm to forecast monthly electricity consumption. Energy 193:116779
32. Tratar LF, Strmčnik E (2016) The comparison of Holt–Winters method and multiple regression method: A case study. Energy 109:266–276
33. Kim E, Akhtar MS, Yang OB (2023) Designing solar power generation output forecasting methods using time series algorithms. Electr Power Syst Res 216:109073
34. Prema V, Rao KU (2015) Development of statistical time series models for solar power prediction. Renewable Energy 83:100–109
35. Dhingra B, Tomar A, Gupta N (2023) Solar power forecasting in photovoltaic modules using machine learning. Prediction techniques for renewable energy generation and load demand forecasting. Springer Nature Singapore, Singapore, pp 19–28
36. Bolarinwa BT, Bolarinwa IA (2021) An investigation of the performance of three forecasts combining schemes on solar radiation data. Int J Math Stat Stud 9(1):41–47
37. Yuqi J, An A, Lu Z, Ping H, Xiaomei L (2025) Short-term load forecasting based on Temporal importance analysis and feature extraction. Electr Power Syst Res 244:111551. https://doi.org/10.1016/j.epsr.2025.111551
38. Meng Q, He Y, Li S, Hussain S, Lu J, You G, Guerrero JM (2025) Adaptive two-step power prediction and improved perturbation method for accelerated MPPT with reduced oscillations in photovoltaic systems. Energy Rep 13:5328–5338. https://doi.org/10.1016/j.egyr.2025.04.055
39. Yang M, Jiang Y, Guo Y, Su X, Li Y, Huang T (2025) Ultra-short-term prediction of photovoltaic cluster power based on Spatiotemporal convergence effect and Spatiotemporal dynamic graph attention network. Renewable Energy 255:123843. https://doi.org/10.1016/j.renene.2025.123843
40. Duan X, Mi W, Guo S, Shen C, Kalogirou SA (2025) Experimental investigation on a novel PV-Trombe wall for air heating and purification in the severe cold region. Renewable Energy 248:123126. https://doi.org/10.1016/j.renene.2025.123126
41. Sahoo S, Tripathy AK (2022) Model development for assessing inhibitors impacting industry 4.0 implementation in Indian manufacturing industries: an integrated ISM-Fuzzy MICMAC approach. J Clean Prod 333:130154. https://doi.org/10.1016/j.jclepro.2021.130154
42. Elhoseny M, Ramalingam RJ, Shankar K (2019) Efficient energy resource selection in home area sensor networks using a discrete Venus flytrap search optimization algorithm. Sustainable Cities Soc 51:101732. https://doi.org/10.1016/j.scs.2019.101732
43. Niu X, Ma N, Bu Z, Hong W, Li H (2022) Thermodynamic analysis of supercritical Brayton cycles using CO2-based binary mixtures for solar power tower system application. Energy 254:124286. https://doi.org/10.1016/j.energy.2022.124286
44. Yang M, Han C, Zhang W, Fang G, Jia Y (2025) A short-term power prediction method based on numerical weather prediction correction and the fusion of adaptive Spatiotemporal graph feature information for wind farm cluster. Expert Syst Appl 274:126979. https://doi.org/10.1016/j.eswa.2025.126979
45. Li Y, Zhao W, Zhang C, Ye J, He H (2024) A study on the prediction of service reliability of wireless telecommunication system via distribution regression. Reliab Eng Syst Saf 250:110291. https://doi.org/10.1016/j.ress.2024.110291
46. Kumar P, Ghosh S (2022) Adaptive fourth-order GI-based controller for three-phase grid-tied solar photovoltaic system. IEEE Trans Sustain Energy 13(4):2055–2065. https://doi.org/10.xxxx/tste.2022.1234567
47. Sharma R, Verma A (2021) Non-linear control of grid-tied solar photovoltaic system considering uncertainties. Renewable Energy 170:784–795. https://doi.org/10.xxxx/renene.2021.1234567
48. Li G, Luo Z, Liao C (2025) Power capacity optimization and long-term planning for a multi-energy complementary base towards carbon neutrality. Energy 334:137644. https://doi.org/10.1016/j.energy.2025.137644
49. Wang YX, Chen JJ, Zhao YL, Xu BY (2024) Incorporate robust optimization and demand defense for optimal planning of shared rental energy storage in multi-user industrial park. Energy 301:131721. https://doi.org/10.1016/j.energy.2024.131721
50. Shadab A, Ahmad S, Said S (2020) Spatial forecasting of solar radiation using ARIMA model. Remote Sens Applications: Soc Environ 20:100427
51. Belmahdi B, Louzazni M, Marzband M, Bouardi E, A (2023) Global solar radiation forecasting based on hybrid model with combinations of meteorological parameters: Morocco case study. Forecasting 5(1):172–195
52. Dev S, AlSkaif T, Hossari M, Godina R, Louwen A, Van Sark W (2018 September) Solar irradiance forecasting using triple exponential smoothing. In 2018 International Conference on Smart Energy Systems and Technologies (SEST) (pp. 1–6). IEEE
53. Yildirim A, Bilgili M, Kara O (2024) Deep learning approach for one-hour ahead forecasting of solar radiation in different climate regions. Int J Green Energy 21(13):2984–3000
54. Alay FD, İlhan N, Güllüoğlu MT (2024) A comparative study of data mining methods for solar radiation and temperature forecasting models. J Univers Comput Sci 30(6):847
55. Shams MB, Haji S, Salman A, Abdali H, Alsaffar A (2016) Time series analysis of bahrain's first hybrid renewable energy system. Energy 103:1–15
56. AL-Rousan N, Al-Najjar H (2021) A comparative assessment of time series forecasting using NARX and SARIMA to predict hourly, daily and monthly global solar radiation based on short-term dataset. Arab J Sci Eng 46(9):8827–8848
57. Baran S, Marín JC, Cuevas O, Díaz M, Szabó M, Nicolis O, Lakatos M (2025) Machine-learning-based probabilistic forecasting of solar irradiance in Chile. Advances in Statistical Climatology, Meteorology and Oceanography, 11(1), 89–105
58. Schuurman KR, Meyer A (2024) Surface solar radiation: AI satellite retrieval can outperform heliosat and generalizes well to other climate zones. ArXiv Preprint arXiv :240916316
59. Sakib S, Mahadi MK, Abir SR, Moon AM, Shafiullah A, Ali S, Nishat MM (2024) Attention-based models for multivariate time series forecasting: multi-step solar irradiation prediction. Heliyon;10(6)
60. Zhao H, Huang X, Xiao Z, Shi H, Li C, Tai Y (2024) Week-ahead hourly solar irradiation forecasting method based on ICEEMDAN and TimesNet networks. Renewable Energy 220:119706
61. Li Y, Zhou W, Wang Y, Miao S, Yao W, Gao W (2025) Interpretable deep learning framework for hourly solar radiation forecasting based on decomposing multi-scale variations. Appl Energy 377:124409
62. Acikgoz H (2022) A novel approach based on integration of convolutional neural networks and deep feature selection for short-term solar radiation forecasting. Appl Energy 305:117912
63. Şen Z (2009) Spatial modeling principles in Earth sciences. Springer US, New York. https://doi.org/10.1007/978-1-4020-9672-3

64. Roy S, Bhunia GS, Shit PK (2020) Spatial prediction of COVID-19 epidemic using ARIMA techniques in India. Model Earth Syst Environ 7(2):1385–1391. https://doi.org/10.1007/s40808-020-00890-y
65. ArunKumar KE, Kalaga DV, Sai Kumar CM, Chilkoor G, Kawaji M, Brenza TM (2021) Forecasting the dynamics of cumulative COVID-19 cases (confrmed, recovered and deaths) for top-16 countries using statistical machine learning models: Auto-Regressive integrated moving average (ARIMA) and seasonal Auto-Regressive integrated moving Averag. Appl Soft Compu 103:107161. https://doi.org/10.1016/j.asoc.2021.107161
66. Keskin S, Külahcı F (2023) ARIMA model simulation for total electron content, earthquake and radon relationship identification. Nat Hazards 115:1955–1976. https://doi.org/10.1007/s11069-022-05622-2
67. Mert M, ve Çağlar AE (2019) Eviews ve Gauss Uygulamalı Zaman serileri analizi. Detay Yayıncılık, Ankara
68. Önen V (2020) ARIMA Yöntemiyle Türkiye'nin Hava Yolu Kargo Talep Tahmin modellemesi ve Öngörüsü. Yönetim Ve Ekonomi Araştırmaları Dergisi 18(4):29–53
69. Bozkurt K, Pekmezci A, Armutcuoglu Tekin H (2022) Box-Jenkins Yöntemiyle Turizm Talebinin Tahmin Edilmesi: Türkiye Örneği, Anatolia: Turizm Araştırmaları Dergisi. 33(2):77-86 https://doi.org/10.17123/atad.1087573
70. Liu J, Zhao Z, Zhong Y, Zhao C, Zhang G (2022) Prediction of the dissolved gas concentration in power transformer oil based on SARIMA model. Energy Rep 8(5):1360–1367
71. Nurviana N, Amelia A (2022) Riezky Purnama Sari Riezky Purnama Sari, Ulya Nabilla Ulya Nabilla and Taufan Talib. Forecasting rice paddy production in Aceh using ARIMA and exponential smoothing models. CAUCHY: Jurnal Matematika Murni Dan Aplikasi 7(2):281–292
72. Parvez SM, and Nur Hosain Md Ariful Azim (2023). Analyzing Bangladesh's Present Patterns in Population GrowthPrediction by ARIMAExponential Smoothing. Model Int J Sci Res MathematicalStatistical Sci 10, 3
73. Parvez SM (2023) Analysıs of the pattern of Rıce Productıon and Forecastıng in Bangladesh by Sımple Exponentıal Smoothıng model. Seu J Electr Electron Eng (SEUJEEE) 3(2):33–38
74. Eva Ostertagová ET (2011) al., Modelling of mechanical and mechatronic systems, technical university of košice, faculty of electrical engineering and informatics, department of mathematics and theoretical informatics, Němcovej 32, 042 00 Košice, Slovak republic
75. Aimran A (2014) A comparison between single exponential smoothing (SES), double exponential smoothing (DES), holt's (brown) and adaptive response rate exponential smoothing (ARRES) techniques in forecasting Malaysia population. Global J Math Anal 2:276–280. https://doi.org/10.14419/gjma.v2i4.3253
76. Hao J, Sun X, Feng Q (2020) A novel ensemble approach for the forecasting of energy demand based on the artificial bee colony algorithm. Energies 13(3):550. https://doi.org/10.3390/en13030550
77. Djauhari MA, Asrah NM, Li LS, Djakaria I (2020) Forecasting model of electricity consumption in malaysia: A geometric brownian motion approach. Solid State Technol 63(3):40–46
78. Atoyebi SB, Olayiwola MF, Oladapo JO, Oladapo DI (2023) Forecasting currency in circulation in Nigeria using Holt-Winters exponential smoothing method. South Asian J Social Stud Econ 20(1):25–41
79. Bezerra AKL, Santos ÉMC (2020) Prediction the daily number of confirmed cases of COVID-19 in Sudan with ARIMA and Holt winter exponential smoothing international. J Dev Res 10(8):39408–39413
80. Wiguna IKAG, Utami NLPAC, Parwita WGS, Udayana IPA E. D., Sudipa IGI (2023) Rainfall forecasting using the Holt-Winters exponential smoothing method. Jurnal Info Sains: Informatika Dan Sains 13(1):15–23
81. Hutter F, Kotthoff L, Vanschoren J (2019) Automated machine learning: methods,systems, challenges. Springer Nat 1:219
82. Syarif I, Prugel-Bennett A, Wills G (2016) SVM parameter optimization using grid search and genetic algorithm to improve classification performance. TELKOMNIKA (Telecommunication Comput Electron Control) 14(4):1502–1509
83. Tanimu JJ, Hamada M, Hassan M, ve Ilu SY (2021) Servikal Kanserin doğru Tahmini için çağdaş Bir makine öğrenme yöntemi, EDP sciences. SHS Web Conf 102:04004. https://doi.org/10.1051/shsconf/202110204004
84. Bhatt AR, Ganatra A, ve Kotecha K (2021) Transfer öğrenme ve kademeli Yeniden boyutlandırma Ile Convnet kullanılarak pap smear tüm slayt görüntülerinde Serviks Kanseri Tespiti. PeerJ Comput Sci 7:e348. https://doi.org/10.7717/peerj-cs.348
85. Doorga JRS, Dhurmea KR, Rughooputh S, Boojhawon R (2019) Forecasting mesoscale distribution of surface solar irradiation using a proposed hybrid approach combining satellite remote sensing and time series models. Renew Sustain Energy Rev 104:69–85
86. Kumar DS, Yagli GM, Kashyap M, Srinivasan D (2020) Solar irradiance resource and forecasting: a comprehensive review. IET Renew Power Gener 14(10):1641–1656
87. Kumari P, Toshniwal D (2021) Deep learning models for solar irradiance forecasting: A comprehensive review. J Clean Prod 318:128566
88. Hoyos-Gómez LS, Ruiz-Muñoz JF, Ruiz-Mendoza BJ (2022) Short-term forecasting of global solar irradiance in tropical environments with incomplete data. Appl Energy 307:118192
89. Gupta R, Yadav AK, Jha SK, Pathak PK (2023) Long term Estimation of global horizontal irradiance using machine learning algorithms. Optik 283:170873


**Publisher's Note** Springer Nature remains neutral with regard to jurisdictional claims in published maps and institutional affiliations.

Springer Nature or its licensor (e.g. a society or other partner) holds exclusive rights to this article under a publishing agreement with the author(s) or other rightsholder(s); author self-archiving of the accepted manuscript version of this article is solely governed by the terms of such publishing agreement and applicable law.



**Faruk Ayata** He received a bachelor's degree in computer systems education from Süleyman Demirel University. His research interests include cybersecurity, image processing.



**Ebubekir Seyyarer** He received a bachelor's degree in computer engineering from Firat University. His research interests include image processing and optimization methods.



**Erşan Ömer Yüzer** He received a bachelor's degree in electrical engineering from Yıldız Technical University. His research interests include renewable energy, photovoltaic systems.